Department of Biomedical Engineering and Computational Science

Liposome Nanoparticles for Targeted Drug Delivery, Gene Delivery and Magnetic Imaging

SANJEEV RANJAN

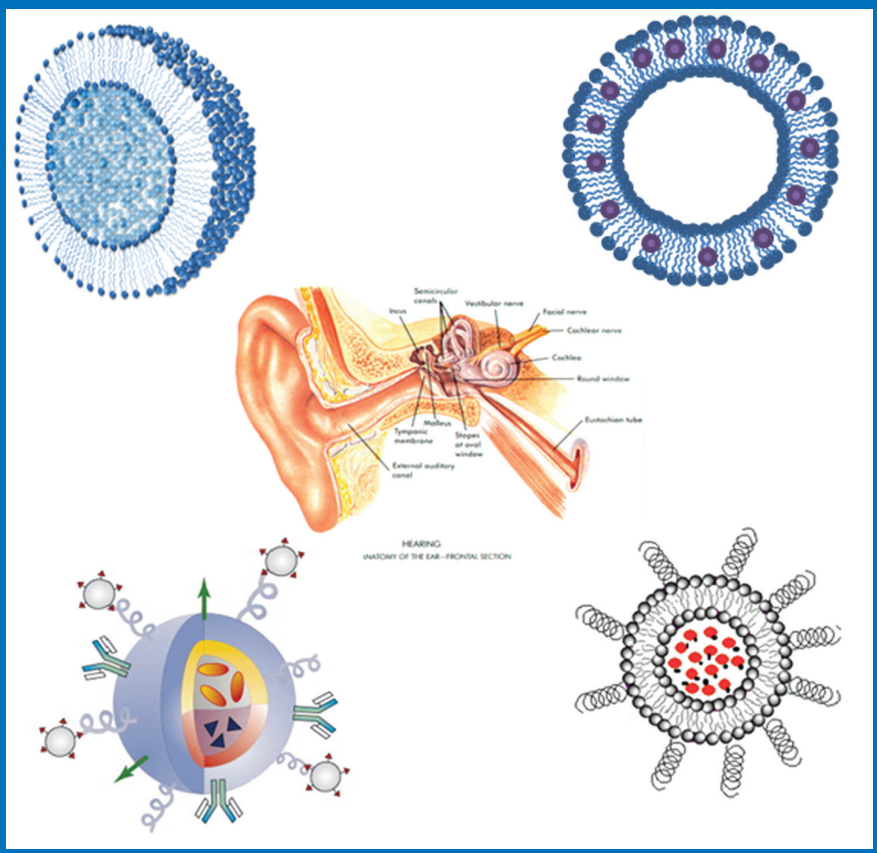

Aalto University

DOCTORAL DISSERTATIONS

Aalto University publication series
DOCTORAL DISSERTATIONS 139/2012

Liposome Nanoparticles for Targeted Drug Delivery, Gene Delivery and Magnetic Imaging

SANJEEV RANJAN

Doctoral dissertation for the degree of Doctor of Science in Technology (Doctor of Philosophy) to be presented with due permission of the School of Science for public examination and debate in Auditorium F239a of the Department of Biomedical Engineering and Computational Science of the Aalto University School of Science (Espoo, Finland) on the 21st of November 2012 at 12 noon.

Aalto University
School of Science
Dept. of Biomedical Engineering and Computational Science
Helsinki Biophysics and Biomembrane Group (HBBG)

Supervising professor
Professor Paavo K. J. Kinnunen
Helsinki Biophysics and Biomembrane Group (HBBG)
Department of Biomedical Engineering and Computational Science
Aalto University School of Science
Finland

Preliminary examiners
Professor Patrick Saulnier
Micro and Therapeutic Nanomedicine
National Institute of Health and Medical Research (INSERM)
&
Faculty of Pharmaceutical Sciences and Health Engineering
University of Angers
France

Adj. Professor Maija Vihinen-Ranta
NanoScience Center
Department of Biological and Environmental Science
University of Jyväskylä
Finland

Opponent
Professor Tommy Nylander
Organizing molecular matter
Department of Chemistry
Lund University
Sweden

Custos
Professor Paavo K. J. Kinnunen,
Aalto University School of Science
Finland

Aalto University publication series
DOCTORAL DISSERTATIONS 139/2012

ISBN 978-952-60-4839-0 (printed)
ISBN 978-952-60-4840-6 (pdf)
ISSN-L 1799-4934
ISSN 1799-4934 (printed)
ISSN 1799-4942 (pdf)
http://urn.fi/URN:ISBN:978-952-60-4838-3

Unigrafia Oy
Helsinki 2012

Finland

441 697
Printed matter

To my parents

Shivajee Roy & Radha Rani Roy

Author
Sanjeev Ranjan

Name of the doctoral dissertation
Liposome Nanoparticles for Targeted Drug Delivery, Gene Delivery and Magnetic Imaging

Publisher School of Science

Unit Department of Biomedical Engineering and Computational Science

Series Aalto University publication series DOCTORAL DISSERTATIONS 139/2012

Field of research Biomedical Engineering and Biophysics

Manuscript submitted 20 August 2012 **Date of the defence** 21 November 2012

Permission to publish granted (date) 11 October 2012 **Language** English

☐ **Monograph** ☒ **Article dissertation (summary + original articles)**

Abstract

Liposomes are spherical vesicles with an aqueous inner cavity surrounded by a lipid bilayer membrane. Liposomes of around 100 nm mean diameter can be classified as nanoparticles (we here refer to liposomes of this size as liposome nanoparticles). Liposome nanoparticles exhibit several properties such as ultra small-size, large surface-area-to-mass ratio, and high reactivity, all of which may be useful in various applications. The small diameter of the liposome nanoparticles is an important attribute that enables them to pass various in vivo barriers for systemic delivery. The present study aimed at developing multifunctional liposomes to deliver drugs and genes with peptide-driven targetability and MRI visualisation to treat inner ear disorders. In addition to the fact that liposomes can be targeted to selected cell populations, they are biodegradable, traceable in vivo, and can be used for controlled drug release.

The first aim of the present study was to develop a method to prepare liposomes with diameter less than 100 nm using a novel procedure, adaptive focused ultrasound (AFU). AFU has several advantages compared to other ultrasound-based techniques; it is non-invasive and isothermal, and the energy involved is much more precisely controlled owing to focusing of the acoustic energy.

The development of new methods for the efficient delivery of drugs to the inner ear represents an important step towards the treatment of cochlear diseases and injury and the amelioration of hearing loss. The second aim of this project was to analyse the efficacy of the penetration of liposomes through the round window membrane when injected into the middle ear cavity in mice and to determine whether the accumulation of liposomes in the inner ear tissues after such treatment were sufficient to elicit a therapeutic response. Our results demonstrate that liposomes are capable of carrying into the inner ear a drug, disulfiram that elicits a biological effect that is measurable by a functional readout.

As its third aim, this study investigated the selective targetability of inner ear neuronal cells using the survival receptor tyrosine kinase B (TrkB) for targeted gene delivery. We demonstrate the feasibility of targeting of liposomes to TrkB-expressing cells by designed peptides that promote cellular uptake via receptor-mediated pathways.

Our fourth aim was to track the dynamics and distribution of liposomes in vivo by preparing MRI-traceable liposomes. Effective MRI-traceable liposomes were developed by encapsulating gadolinium, which was visualised in vivo in the rat inner ear using a 4.7 T MR machine. The dynamics were correlated to the status of the perilymph circulation.

Keywords Liposome, Nanoparticles, Inner ear, Ultrasound, Drug, Gene, Disulfiram, Peptide, MRI

ISBN (printed) 978-952-60-4839-0 **ISBN (pdf)** 978-952-60-4840-6

ISSN-L 1799-4934 **ISSN (printed)** 1799-4934 **ISSN (pdf)** 1799-4942

Location of publisher Espoo **Location of printing** Helsinki **Year** 2012

Pages 137 **urn** http://urn.fi/URN:ISBN:978-952-60-4838-3

Tekijä
Sanjeev Ranjan

Väitöskirjan nimi
Liposominanopartikkeleita kohdennettua lääkeaineiden ja geenien toimitusta ja magneettikuvantamista varten

Julkaisija Aalto-yliopiston perustieteiden korkeakoulu

Yksikkö Lääketieteellisen tekniikan ja laskennallisen tieteen laitos

Sarja Aalto University publication series DOCTORAL DISSERTATIONS 139/2012

Tutkimusala Lääketieteellinen tekniikka ja biofysiikka

Käsikirjoituksen pvm 20.08.2012 **Väitöspäivä** 21.11.2012

Julkaisuluvan myöntämispäivä 11.10.2012 **Kieli** Englanti

☐ **Monografia** ☒ **Yhdistelmäväitöskirja (yhteenveto-osa + erillisartikkelit)**

Tiivistelmä

Liposomit ovat pallomaisia vesikkeleitä, joiden sisällä olevaa vesiliuosta ympäröi lipidikaksoiskalvo. Halkaisijaltaan n. 100 nm:n liposomit voidaan luokitella nanopartikkeleiksi (s.o. liposominanopartikkeleiksi). Liposominanopartikkeleilla on useita hyödyllisiä ominaisuuksia: ultrapieni koko, suuri pinta-ala suhteessa massaan ja suuri reaktiivisuus. Liposomien pieni halkaisija on tärkeä ominaisuus systeemisen käytön kannalta, sillä se mahdollistaa monien esteiden välttämisen tai läpäisyn in vivo: veren komponenttien ohittamisen, kasvaimiin pääsyn, retikuloendoteliaalijärjestelmän, soluväliaineen komponenttien ohittamisen ja solunsisäisten esteiden läpäisyn. Väitöskirjatyössä kehitettiin sisäkorvan sairauksien hoitoa varten multifunktionaalisia liposomeja, joilla voidaan toimittaa lääkeaineita ja geenejä sisäkorvaan ja jotka voidaan visualisoida magneettikuvauksella.

Tutkimuksen ensimmäisenä tavoitteena oli <100 nm halkaisijaltaan olevien liposomien tuottaminen uudella, adaptiivista fokusoitua ultraääntä (AFU) hyödyntävällä tekniikalla. Muihin ultraäänimenetelmiin verrattuna etuna on, ettei menetelmä ole invasiivinen, prosessi voidaan toteuttaa vakiolämpötilassa ja akustisen energian fokusoinnin vuoksi prosessia voidaan kontrolloida tarkemmin.

Uusien menetelmien kehittäminen lääkeaineiden tehokkaaseen sisäkorvaan kuljettamiseen on tärkeää sisäkorvan sairauksien ja vaurioiden hoitamiseksi ja kuulohäiriöiden lievittämiseksi. Toisena tavoitteena oli selvittää, miten tehokkaasti välikorvaan injisoidut liposomit pääsevät sisäkorvaan pyöreän ikkunan läpi ja saadaanko sisäkorvaan näin tarpeeksi suuria pitoisuuksia terapeuttisen vasteen saamiseksi. Tulokset osoittavat liposomien pystyvän kuljettamaan tarpeeksi lääkeainetta (disulfiraamia) sisäkorvaan biologisen vasteen tuottamiseksi; vaste oli havaittavissa toiminnallisissa mittauksissa.

Kolmantena tavoitteena oli tutkia, miten sisäkorvan neuronien hengissä säilymistä ylläpitävän tyrosiinikinaasi B:tä (TrkB:n) voitaisiin käyttää geenien kuljettamisessa valikoidusti näihin neuroneihin. Työssä osoitettiin, että liposomien pinnalla olevien peptidien avulla voidaan reseptorivälitteisten reittien kautta suunnata liposomien ottoa TrkB:tä ilmentäviin soluihin.

Neljäntenä tavoitteena oli seurata liposomien jakautumista ja dynamiikkaa in vivo magneettikuvantamisella. Liposomeihin sisällytettiin gadoliniumia, jotta liposomeja voitiin jäljittää magneettikuvantamisella in vivo rottien sisäkorvassa 4,7 Teslan magneettikuvantamislaitteella. Liposomien kierto korreloi perilymfan kierron kanssa.

Avainsanat liposomi, nanopartikkeli, sisäkorva, ultraääni, geeni, disulfiraami, peptidi, magneettikuvantaminen

ISBN (painettu) 978-952-60-4839-0 **ISBN (pdf)** 978-952-60-4840-6

ISSN-L 1799-4934 **ISSN (painettu)** 1799-4934 **ISSN (pdf)** 1799-4942

Julkaisupaikka Espoo **Painopaikka** Helsinki **Vuosi** 2012

Sivumäärä 137 **urn** http://urn.fi/URN:ISBN:978-952-60-4838-3

Preface

The research presented in this thesis was conducted at the *Helsinki Biophysics and Biomembrane Group, Institute of Biomedicine, Faculty of Medicine, University of Helsinki* during the years 2006-2010 and in the *Department of Biomedical Engineering and Computational Science, Aalto University School of Science* during the years 2010-2012. I had the opportunity to work in a European Union project, "NANOEAR", the aim of which is to develop various types of nanoparticles for treatment of inner ear disorders.

First of all, I would like to thank my supervisor, Professor Paavo Kinnunen, for welcoming me into his group six years ago when I was still a Master student and for giving me the opportunity to pursue a Ph.D. His help, guidance and constant enthusiasm have been very much appreciated during the past years. I am also very grateful to Professor Ilmari Pyykkö of the *University of Tampere Medical School* for being such a wonderful project coordinator.

I wish to thank all the NANOEAR consortium members from different universities of Europe. To my co-authors, I express my thanks for their collaboration and kind interest. I especially thank Dr. Jiří Popelář of the *Academy of Sciences of the Czech Republic*, Dr. Jing Zou of the *University of Tampere* and Dr. Jozsef Dudas of the *Innsbruck Medical University, Austria*.

My warm thanks and gratitude to the external reviewers of this thesis, Professor Patrick Saulnier (*University of Angers, France*) and Adj. Professor Maija Vihinen-Ranta (*University of Jyväskylä, Finland*), for their availability and feedback. Professor Tommy Nylander (*Lund University, Sweden*) is deeply thanked for accepting the role of an opponent. It is my honour to have him as an opponent.

I am indebted to Rohit Sood, who was so helpful at the start of my project. Later on, we worked together on the NANOEAR project. It was always a great pleasure to discuss the project with him, planning experiments and

going abroad for the project meetings. I owe a thousand thanks to him. I extend my thanks to the other members of the group and, in no particular order, I would like to thank Roberto, Juha-Matti, Vladimir, Aqeel, Chris, and Roman, as well as all the other present and past members of the group (Juha-Pekka, Karen, Yegor, Mikko, Sonia and Pavol) and visiting scientists for making the last five years such an enriching experience. I will certainly miss our endless discussions in the coffee room.

I also wish to express my gratitude to my previous mentors, Dr. P. Chattopadhyay, Addl. Professor, *All India Institute of Medical Sciences*, *New Delhi*, my mentor during my undergraduate studies, and Dr. Pravindra Kumar, Asst. Professor, *Indian Institute of Technology*, *Roorkee*, my master's thesis supervisor and mentor.

Many thanks to Saroj Kumar, Saket Saurabh, Kapil Dev and Vinay Sagar for strengthening and guiding me whenever I needed it. It gives me pleasure to thank my friends: Arun, Shishir, Krishna, Aniket and Anmol for the good times we shared. My stay in Helsinki/Espoo would not have been so pleasant without my friend and labmate Ajay Mahalka, who was always available and helpful.

Heartiest thanks to the most ideal person in my life, my brother Rajeev Ranjan, and to my sister Indu Rani Roy, for always being there for me. I owe a very special thanks to my fiancée Alka for her love and friendship.

This research was supported by a grant from the European Community 6th Framework Programme on Research, Technological Development and Demonstration (Nanotechnology-based Targeted Drug Delivery), European Union FP6 project contract number NMP4-CT-2006-026556. In addition, personal grants from the Magnus Ehrnrooth foundation, The National Doctoral Programme in Nanoscience, and The National Graduate School of Organic Chemistry and Chemical Biology are gratefully acknowledged. Numerous travel grants have been awarded to enable me to present my work at different international conferences in Europe, the USA and Japan.

Finally, I am extremely grateful to the Finland Otolaryngologist Association for honouring me with the Dissertation Fellowship Award of 2012.

Helsinki, October 12th 2012
Sanjeev Ranjan

Liposome Nanoparticles for Targeted Drug Delivery, Gene Delivery and Magnetic Imaging

List of original publications

This thesis consists of an overview and the following publications, which are referred to in the text by their Roman numerals:

I **Making Unilamellar Liposomes Using Focused Ultrasound.**
Roberto Tejera-Garcia[§], Sanjeev Ranjan[§], Vladimir Zamotin, Rohit Sood, and Paavo K. J. Kinnunen
Langmuir, 27, 10088-10097, 2011.
§ *First two authors contributed equally to this work*

II **Minimally Invasive Drug Delivery to the Cochlea Through Application of Nanoparticles to the Round Window Membrane.**
Daniela Buckiová, Sanjeev Ranjan, Tracey A. Newman, Alexander H. Johnston, Rohit Sood, Paavo K. J. Kinnunen, Jiří Popelář, Tetyana Chumak, Josef Syka
Nanomedicine (London, England), 7, 1339-1354, 2012.

III **Peptide-Mediated Targeting of Liposomes to TrkB Receptor Expressing Cells.**
Sanjeev Ranjan, Rohit Sood, Jozsef Dudas, Rudolf Glueckert, Anneliese Schrott-Fischer, Soumen Roy, Ilmari Pyykkö, and Paavo K.J. Kinnunen,
International Journal of Nanomedicine, 7, 3475-3485, 2012.

IV **Manufacturing and *in vivo* Inner Ear Visualization of MRI Traceable Liposome Nanoparticles Encapsulating Gadolinium.**
Jing Zou, Rohit Sood, Sanjeev Ranjan, Dennis Poe, Usama Abo Ramadan, Paavo K.J. Kinnunen, Ilmari Pyykkö
Journal of Nanobiotechnology, 8, 32, 2010.

List of other publications

V **Internalization of Liposome Nanoparticles Functionalized With TrkB Ligand in Rat Cochlear Cell Populations.**
Jing Zou, Ya Zhang[†], Weikai Zhang[†], Sanjeev ranjan[†], Rohit Sood, Andrey Mikhailov, Paavo Kinnunen, Ilmari pyykkö, *European Journal of Nanomedicine*, 2, 8-13, 2009.
[†] *Equal Contribution*

VI **Visualization of Intracellular Trafficking of Math1 Protein in Different Cell Types With a Newly-Constructed Nonviral Gene Delivery Plasmid.**
Weikai Zhang, Ya Zhang[†], Rohit Sood[†], Sanjeev Ranjan, Elena Surovtseva, Aqeel Ahmad, Paavo Kinnunen, Ilmari Pyykkö, Jing Zou,
The Journal of Gene Medicine, 13, 134-144, 2011
[†] *Equal Contribution*

VII **Size-Dependent Passage of Liposome Nanocarriers With Preserved Posttransport Integrity Across the Middle-inner Ear Barriers in Rats.**
Jing Zou[†], Rohit Sood[†], Sanjeev Ranjan, Dennis Poe, Usama Abo Ramadan, Ilmari Pyykkö, and Paavo K. J. Kinnunen, *Otology & Neurotology*, 33, 666-73, 2012.
[†] *Equal Contribution*

VIII **Liposome Nanoparticles for Targeted Drug and Gene Delivery and Magnetic Imaging.**
Sanjeev Ranjan
In: Proceed with Caution? Concept and Application of the Precautionary Principle in Nanobiotechnology, Rainer Paslack, Johann S. Ach, Beate Lüttenberg, Klaus-Michael Weltring (Eds.). *LIT Publishing House, Muenster,* 2012

IX **Nanoparticle Based Delivery for Treatment of Inner Ear Disorders.**
Ilmari Pyykkö,(...), Sanjeev Ranjan, et al., submitted in *Advanced Drug Delivery Reviews*, xx, 2012.

X **Novel Endosomolytic Peptides for Enhancing Gene Delivery in Nanoparticles.**
Aqeel Ahmad, Sanjeev Ranjan, Weikai Zhang, Jing Zou, Ilmari Pyykkö and Paavo K. J. Kinnunen
Manuscript

XI **Drug Delivery by Nanoparticles – Facing the Obstacles.**
M. Löbler, H. W. Rohm, K. -P. Schmitz, A. H. Johnston, T. A. Newman, S. Ranjan, R. Sood, and P. K. J. Kinnunen
IFMBE Proceedings, 22, 2335-2338, 2009

Author's contribution

I	First two authors contributed equally to this work. The author, together with the first author, contributed to the design and execution of the experiments, analysis of the data, interpreted the results, and wrote very first draft of the manuscript.
II	The author contributed in the designing and preparation of liposomes and contributed in writing of the manuscript.
III	The author participated in planning the experiments. Targeted liposomes were tested at Innsbruck Medical University. The author contributed to the processing of the data and wrote the very first draft of the manuscript.
IV	The author participated in the designing and preparation of the liposomes.

List of symbols and abbreviations

ABR	auditory brainstem response
AFU	adaptive focused ultrasound
ATRA	all-trans retinoic acid
BDNF	brain-derived neurotrophic factor
Chol	cholesterol
CPB	cycles per burst
Cryo-TEM	cryogenic transmission electron microscopy
DAPI	4', 6-diamino-2-phenylindole dihydrochloride
DC	duty cycle
DIC	differential interference contrast
DLS	dynamic light scattering
DMPE-DTPA (Gd)	1,2-ditetradecanoyl-*sn*-glycero-3-phosphoethanolamine-N-diethylenetriaminepentaacetic acid (gadolinium salt)
DOPE	1, 2-distearoyl-*sn*-glycero-3-phosphoethanolamine
DPPC	1,2-dipalmitoyl-*sn*-glycero-3-phosphocholine
DPPG	1,2-dipalmitoyl-*sn*-glycero-3-phospho-(1'-*rac*-glycerol)
DPPRho	1,2-dipalmitoyl-*sn*-glycero-3-phosphoethanolamino-thiocarbamoyl-N-6-tetramethylrhodamine
DSC	differential scanning calorimetry
DSPE-PEG-2000	1,2-distearoyl-*sn*-glycero-3-phosphoethanolamine-N-[methoxy(polyethylene glycol)-2000] (ammonium salt)
DSPE-PEG(2000)maleimide	1,2-distearoyl-sn-glycero-3-phosphoethanolamine-N-[(polyethylene glycol)-2000 maleimide]
EDTA	ethylenediaminetetraacetic acid
EGFP	enhanced green fluorescent protein
EggPC	phosphatidylcholine from egg yolk
FACS	fluorescence activated cell sorting
FITC	fluorescein isothiocyanate
FOV	field of view
Gd	gadolinium, gadolinium chelate

Gd-DOTA	gadolinium-tetra-azacyclo-dodecane-tetra-acetic acid
Hepes	N-2-hydroxyethylpiperazine-N-2-ethanesulfonic acid
HPLC	high-performance liquid chromatography
IgG	immunoglobulin G
LUV	large unilamellar vesicles
LysoPC	1-stearoyl-2-hydroxy-*sn*-glycero-3-phosphocholine
MLV	multilamellar vesicles
MR	magnetic resonance
MRI	magnetic resonance imaging
NBD	nitro-2-1,3-benzoxadiazol-4-yl
NBD-PC	1-hexanoyl-2-[6-[(7-nitro-2-1,3-benzoxadiazol-4-yl)amino]hexanoyl]-*sn*-glycero-3-phosphocholine
NEX	number of excitation
NTRK1	gene coding for neurotrophic tyrosine kinase receptor TrkA
NTRK2	gene coding for neurotrophic tyrosine kinase receptor TrkB
PBF	phospholipid bilayer fragments
PCL	peptide-conjugated liposomes
PDI	polydispersity index
PEG	polyethylene glycol
POPG	1-palmitoyl-2-oleoyl-*sn*-glycero-3-[phospho-*rac* - (1-glycerol)]
RARE	rapid acquisition with relaxation enhancement
RWM	round window membrane
SDS	sodium dodecyl sulfate
SG	spiral ganglion
SM	scala media
SOPC	1-stearoyl-2-oleoyl-*sn*-glycero-3-phosphocholine
SPECT	single-photon emission computed tomography
Sph	sphingosine
ST	scala tympani,
SUV	small unilamellar vesicles
SV	scala vestibule
TeV	tobacco etch virus
TFA	trifluoroacetic acid
T_m	main phase transition temperature
TRITC-DHPE	N-(6-tetramethylrhodaminethiocarbamoyl)-1,2-dihexadecanoyl-*sn*-glycero-3-phosphoethanolamine
TrkA	tyrosine receptor kinase A
TrkB	tyrosine receptor kinase B
Z_{av}	average hydrodynamic particle diameter

1. Introduction

Liposomes, phospholipid vesicles with a bilayered membrane structure, have received a great deal of attention during the past 35 years as pharmaceutical carriers of great potential. Today, several liposome formulations have been commercialised, and others are in various stages of clinical trials. Liposomes in the nanoscale range, especially multifunctional liposomes, have advantages over traditional liposomes for use in nanomedicine, which is the application of nanotechnology to medicine. Nanomedicine concerns the use of precisely engineered materials at nanometer scale (nanoparticles) in the development of novel therapeutic and diagnostic modalities [Wagner et al. 2006].

Nanoparticles have unique physicochemical properties such as ultra-small size, large surface-area-to-mass ratio, and high reactivity that differ from those of bulk materials of the same composition [Zhang 2008]. As a particle's size decreases, a greater proportion of its atoms are located on the surface relative to its core, often rendering the particle more reactive. In addition, the specific surface area of the particle increases exponentially. This reduction in the particle size increases its dissolution rate and saturation solubility and, if the particle is a drug, it frequently correlates with improved *in vivo* drug performance. These properties can be used to overcome some of the limitations encountered in the use of traditional therapeutic and diagnostic agents. Liposomes are the most commonly used nanoparticles in medicine and biology because they are composed of the same material as cell membranes. Various types of liposomes are currently in use clinically as delivery systems for anticancer drugs and vaccines. However, the use of nanoparticles as cell-specific delivery systems is still in the preclinical development stage and represents an emerging field in nanomedicine.

In the present thesis, liposomes have been used for targeted drug delivery, gene delivery and magnetic imaging using the inner ear as a model target organ. Inner ear disease is a significant problem, with hearing loss affecting as many as 44 million people within the European Union alone. According to the World Health Organisation, in 2004 hearing loss and deafness affected at least 275 million people worldwide. Strategies to prevent hearing

loss are limited, and conventional systemic drug delivery to the cochlea is difficult due to the presence of the cochlea-blood barrier.

The cochlea of the inner ear is the most critical structure in the auditory pathway because it is there that the energy from sonically generated pressure waves is transformed into neural impulses. The inner ear is a clinically vital target, well representing the central nervous system and other difficult-to-access body sites; it is isolated and multicompartmental, has neural, supporting and vascular targets, and is relatively immunoprivileged [Nanoear 2011]. There are two openings, the round window and the oval window, between the middle ear and the inner ear. Permeability of a substance through the round window requires passage through two epithelial cell layers and a central connective tissue layer. There is evidence that active transport of smaller nanoparticles through the epithelium occurs via endocytosis, while pinocytosis of larger particles occurs, and both small and micron-sized particles may pass through intercellular channels [Goycoolea 1997]. The intercellular spaces between epithelial cells are 6–8 nm [Balda and Matter 1998], and the tight junction pores are 0.6 nm [Spring 1998]. Therefore, the passage of large molecules requires active and selective opening of the junctions, regulated by structural and signalling molecules [Tsukita 1999]. Nanoparticles and molecules less than 25 nm in diameter [Goycoolea 1997] show increasing permeability with smaller size and may primarily be transported by cholesterol-dependent non-clathrin, non-caveolae endocytosis [Knorr 2007]. Thus, choice of an appropriate delivery method is necessary for efficient distribution of therapeutic agents in the inner ear while minimising adverse effects.

Nanoparticles have been demonstrated to have significant potential for site-selective delivery of drugs and genetic material to the inner ear for the prevention and treatment of injuries and diseases [Poe and Pyykkö 2011]. Targeting of the nanoparticles requires the identification of suitable ligands for receptors that are selectively expressed within the target tissue. There are no or only a few literature reports available on targeted inner ear drug or gene delivery using nanoparticles.

In the process of optimising the functionalisation of nanoparticles for use in treating the inner ear, it is essential to trace their passage through the cochlea. It is problematic to track functionalised nanoparticles in the inner ear by histological means. Magnetic resonance imaging (MRI) is an excellent tool for use in tracing nanoparticles labelled with a contrast agent through the inner ear because it can detect their signal changes in both the inner ear fluids and soft tissue *in vivo*.

The research performed for this thesis is of a multidisciplinary nature. The design and development of multifunctional liposomes is a special focus of this work. The thesis will open with a brief review of the literature related to the four main areas covered by the thesis, namely liposome preparation, liposome-mediated drug delivery, liposomes in gene delivery and magnetic imaging. This will be followed by a statement of the aims of the present study and thereafter by a description of the materials and methods used. In the next section, results and discussion will be presented together. The last part of the thesis will present conclusions and future perspectives.

2. Review of the Literature

2.1 Liposomes

A liposome is defined as a spherical vesicle with an aqueous inner cavity surrounded by a lipid bilayer membrane. Liposomes can be made of naturally derived phospholipids (molecules that comprise cell membranes) with mixed acyl chains (like egg phosphatidylcholine) or of synthetic lipids. The name liposome is derived from two Greek words, 'lipid' meaning fat and 'soma' meaning body. Liposomes were discovered in 1961 by Alec D. Bangham, and their discovery was published in 1964 [Bangham and Horne 1964]. The term 'liposome' does not in itself denote any size characteristics and is not an alternative to the term 'liposome nanoparticle'. Furthermore, the term 'liposome' does not mean that the particle must contain lipophobic contents, such as water (although it usually does).

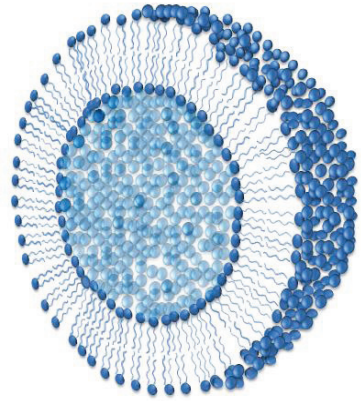

Figure 1.1: Schematic illustration of a liposome, depicting the lipid bilayer and aqueous inner cavity.

2.2 Mechanism of vesicle formation

Liposomes or lipid vesicles are formed when thin lipid films are hydrated and stacks of liquid crystalline bilayers become fluid and swell [Lasic 1988]. Liposome formation requires layer separation and bending. In the early stage of liposome formation, the normal forces that cause repulsion between lipid layers and the tangential forces that bend the lipid layers play

a crucial role [Bagatolli et al. 2000]. The hydrated lipid sheets detach during agitation and self-close to form large multilamellar vesicles (MLV), which prevents interaction of water with the hydrocarbon core of the bilayer at the edges. Once these particles have formed, reduction of the size of the particle requires energy input in the form of sonic energy (i.e., sonication) or mechanical energy (i.e., extrusion).

2.3 Methods for liposome preparation

2.3.1 Sonication: Disruption of MLV suspensions using sonication typically produces small unilamellar vesicles (SUV) with diameters in the range of 15-50 nm [Johnson et al. 1971]. The instruments most commonly used for preparation of sonicated particles are bath and probe tip sonicators. Probe tip sonicators deliver high-energy input to the lipid suspension but can also overheat the lipid suspension, often causing oxidation and degradation of phospholipid. Sonication tips also tend to release titanium particles, which must be removed by centrifugation prior to liposome use. For these reasons, bath sonicators are the most widely used instrumentation for the preparation of SUV. Sonication of an MLV dispersion is accomplished by placing a test tube containing the suspension in a bath sonicator (or by placing the tip of a sonicator in the test tube) and sonicating for 5-10 min at a temperature above the phase transition temperature (T_m) of the lipid. As the SUV form the lipid suspension begins to clarify yielding a slightly hazy transparent solution. The haze is due to light scattering caused by residual large particles remaining in the suspension. These particles can be removed by centrifugation to yield a clear suspension of SUV. The mean size and distribution of SUV formed in this way is influenced by the composition and concentration of lipid, temperature, sonication time and power, volume, and sonicator tuning. Additionally, due to the high curvature of their membranes, SUV are inherently unstable and will spontaneously fuse to form larger vesicles when stored below their phase transition temperature.

2.3.2 Ethanol injection: Small-sized liposomes have several advantages as drug delivery systems, and the ethanol injection method is a suitable technique that can be used to cause the spontaneous formation of liposomes with a small average radius. In this method, a stock solution of a phospholipid in ethanol is rapidly injected into aqueous solution depending upon conditions, liposomes are formed. In [1973], Batzri and Korn showed that this method permits the formation of very small liposomes. The solvent

of choice is usually ethanol, but other alcohols can be used considering factors such as toxicity, water-solubility, viscosity and dissolving power of lipids. This method has many advantages: it is fast, easy, reproducible, and there is no need for additional operations such as extrusion, sterilization or sonication. However, the ethanol injection procedure possesses two potential disadvantages. First, the liposome suspension will contain ethanol; this can be removed by dialysis or ultrafiltration. Second, because large volumes of aqueous solution are used, it is necessary to use relatively large amounts of any solute it is desired to trap within the liposomes. It is usually possible, however, to recover water-soluble material from the ultrafiltrate [Batzri and Korn 1973].

2.3.3 Extrusion: Lipid extrusion is a technique in which a lipid suspension is forced through a polycarbonate filter with a defined pore size to yield particles with diameters near the pore size of the filter [MacDonald et al. 1991]. Prior to extrusion through the filter of choice, MLV suspensions are disrupted either by several freeze-thaw cycles or by pre-filtering the suspension through a membrane with larger pore size (typically 0.2μm-1.0μm). This method helps prevent the membranes from fouling and improves the homogeneity of the size distribution of the final suspension. As with all procedures for downsizing MLV dispersions, the extrusion should be performed at a temperature above the lipid transition temperature of the lipid(s) used to construct the particle. Attempts to extrude below the T_m will be unsuccessful because the membrane has a tendency to become fouled with particles that cannot pass through the pores. Extrusion through filters with 100-nm pores typically yields large unilamellar vesicles (LUV) with mean diameter of 120-140 nm. Mean particle size also depends on lipid composition and is quite reproducible from batch to batch. The drawback of the extrusion method is loss of material in the filters.

Several other techniques are available for preparing liposomes, but each has its limitations. Thus, a method, which must be free from the above problems, is needed to prepare liposomes.

2.4 Liposomes in drug delivery

Liposomes are used for drug delivery owing to their unique properties. A liposome encapsulates a region of aqueous solution inside a hydrophobic membrane; the dissolved hydrophilic solutes cannot readily pass through

the lipids, and hydrophobic chemicals can be dissolved into the membrane. In this way, the liposome can carry both hydrophilic molecules and hydrophobic molecules. Fusion of the lipid bilayer of the liposome with other bilayers such as the cell membrane functions to deliver the liposome contents.

Several procedures for the encapsulation of drugs into liposomes have been described [Defrise et al. 1984]. By preparing liposomes in a solution of drugs that would normally be unable to diffuse through the membrane, drugs can be (indiscriminately) delivered past the lipid bilayer. Liposomes can also be designed to deliver drugs in other ways. Liposomes that contain solutions of low (or high) pH can be constructed such that dissolved aqueous drugs will be charged in solution (i.e., the pH is outside the drug's pI range). Because the pH within the liposome naturally neutralises because protons can pass through a membrane, the drug will also be neutralised, allowing it to freely pass through the liposome membrane [Torchilin et al. 1993]. Liposomes of this type deliver drugs by diffusion rather than by direct cell fusion. Another strategy for liposomal drug delivery is targeting liposomes for endocytosis. Liposomes can be made in a size range that makes them vulnerable to natural macrophage phagocytosis. These liposomes can be digested within the macrophage's phagosome, thus releasing their drug contents. Opsonins and ligands that activate endocytosis in other cell types can also be incorporated into liposome membranes.

Another interesting property of liposomes is their natural ability to target cancer. The endothelial walls of healthy blood vessels are lined by endothelial cells bound together by tight junctions. These tight junctions prevent any large particle in the blood from leaking out of the vessel. However, tumour vessels do not contain the same type of tight junctions between cells and are leaky. This ability is known as the ‘enhanced permeability and retention effect’ [Maeda 2001]. Liposomes of certain sizes, typically less than 400 nm, can rapidly enter tumour sites from the blood but are kept in the bloodstream by the endothelial wall in healthy tissue vasculature. Anti-cancer drugs such as doxorubicin (Doxil) and daunorubicin (Daunoxome) are currently being marketed in liposome delivery systems. Many other liposomal drugs are in clinical trials [Torchilin 2005].

The development of new methods for the efficient delivery of drugs into the inner ear represents an important step towards the treatment of cochlear diseases or injury and the amelioration of hearing loss. Therapeutic surgical approaches or direct drug application to the inner ear

for the treatment of inner ear disorders has limited success and is often accompanied by damaging effects on hearing, balance, and tinnitus levels [McCall et al. 2010] The small diameter of liposome nanoparticles is an important attribute that potentially enables them to overcome various *in vivo* barriers for systemic delivery such as blood components, reticuloendothelial system uptake, tumour access, extracellular matrix components, and intracellular barriers [Li and Szoka 2007].

2.5 Liposomes in gene delivery

Lipoplexes formed by cationic liposomes and nucleic acids are commonly used as nucleic acid delivery systems *in vitro*. Liposome-mediated gene transfer is an attractive method because of its simplicity and low toxicity, and the method holds promise as a potential major breakthrough for use in therapy. Different types of cationic lipids have been used to construct lipoplexes [Subramanian et al. 2000; Säily et al. 2006; Ryhänen et al. 2003]. Some commercially available cationic lipids are DOTMA (N-[1-(2,3-dioleyloxy)propyl]-N,N,N-trimethylammonium chloride), DOTAP (N-(1-(2,3-dioleoyloxy)propyl)-N,N,N-trimethylammonium chloride) and DHAB (dihexadecyldimethylammonium bromide). Compared to viral-based delivery systems, lipoplexes possess a number of desirable properties and have become perhaps the most popular utilities for this purpose [Felgner et al. 1987]. Most importantly, such complexes are nonimmunogenic, nonpathogenic, biodegradable, and easy to prepare. They have also been shown to pass through the blood-brain barrier and are being tested in clinical trials [Shi and Pardridge 2000; Caplen et al. 1995; Alton et al. 1999]. Yet, despite intensive efforts, the mechanism(s) of liposome-mediated transfection (lipofection) and therefore also the characteristics of an ideal transfection agent remain incompletely understood.

Several physical and chemical properties of different cationic lipids have been proposed to be responsible for their ability to transfect cells. Importantly, the number of positive charges on the cationic lipid, the linkage between the hydrophobic and cationic portion of the molecule, and the structure of the hydrophobic moieties have been shown to influence the measured transfection efficiency [Wheeler et al. 1996; Leventis et al. 1990; Solodin et al. 1995]. The properties of specific DNA-cationic lipid complexes have also been extensively studied to determine the composition required for efficient and reproducible transfection. The presence of inverted hexagonal H_{II} phase-forming dioleoylphosphatidylethanolamine (DOPE), diacylglycerol (DAG), or other nonlamellar phase-promoting

compounds in the lipoplex has been demonstrated to enhance transfection efficiency [Farhood et al. 1995; Paukku et al. 1997; de Lima et al. 1999]. However, this requirement is challenged by some previous studies [Hui et al. 1996].

The morphology of cationic lipid-DNA complexes has been visualised by electron microscopy and atomic force microscopy [Wheeler et al. 1996; Sternberg et al. 1994]. These studies suggest the existence of several structures that could be responsible for transfection, including "spaghetti-and-meatballs"-type complexes, dense multilamellar complexes and complexes with particular diameters [Sternberg et al. 1994; Huebner et al. 1999; Kawaura et al. 1998]. However, Xu et al. [1999] reported that the morphology of complexes as visualised by electron microscopy does not have significant impact on their transfection efficiency. Understanding the nature of cationic lipid-DNA interactions could have broader biological significance with respect to the natural cationic lipid sphingosine. The latter is ubiquitously present in mammalian cells and forms complexes with DNA; some of these complexes show "beads-on-a-string" morphology, while others appear as larger aggregates. To this end, the well-established lipid second messenger, phosphatidic acid, is able to reverse DNA-sphingosine complex formation [Kinnunen et al. 1993]. The use of gemini surfactants as transfection vectors has been investigated [Singh et al. 2012; Donkuru et al. 2010; Fielden et al. 2001]. According to Ryhänen et al. [2003], the surface charge density of cationic gemini surfactant determines the efficiency of transfection. Our own unpublished data shows high transfection of immune cells using a class of gemini surfactant as transfection vector [*manuscript in preparation*].

Lipid-based nanoparticles that differ from lipoplexes are currently actively used as gene delivery carriers. These nanoparticles are vesicles composed of lipids and encapsulated nucleic acids and have diameters of approximately 100 nm. The major factors that impact the diameter and encapsulation efficiency of DNA-containing nanoparticles include the lipid composition, nucleic acid-to-lipid ratio and formulation method [Li and Szoka 2007].

To pack and deliver genes noninvasively into the inner ear, several important criteria must to be met. These criteria include round window membrane (RWM) penetration of the vector and cargo, uniform diffusion and distribution of the vector in the treated area, safety with respect to insertional mutagenesis, low toxicity, and cell-specific targetability. In these aspects, liposomes offer the potential to confer an overall positive charge to the desired nucleic acid and thus enhance its transcellular transport.

Several molecular targets are available for inner ear therapy. The tropomyosin receptor kinase B (TrkB) receptor on spiral ganglion (SG) and vestibular hair cells is an especially attractive target [Bitsche et al. 2011]. Although a number of studies have reported an effect of surface functional ligands/motifs on nanocarrier cellular uptake, the impact of ligand density and arrangement on the nanoparticle surface is poorly understood. The organisation and density of surface motifs are likely important in internalisation. Better design of targeting ligands and optimisation of ligand presentation on the surface of liposomes may improve the efficacy of therapeutic liposomes in targeted gene/drug delivery. Such optimal design allows the delivery of therapeutic agents to defined tissue sites, while producing minimal undesired effects elsewhere.

2.6 Liposomes in imaging

Many advanced molecular imaging agents are currently being investigated at the pre-clinical level. Liposomes, in particular, have proven to be very promising carrier systems for diagnostic agents used in single-photon emission computed tomography (SPECT) and MRI, as well as for therapeutic agents to treat diseases such as cancer. Nanosized liposomes have been designed and labelled with the radionuclide holmium-166 (both a beta- and gamma-emitter and also highly paramagnetic) or technetium-99 and co-loaded with paramagnetic gadolinium, allowing multimodality SPECT and MRI and radionuclide therapy with a single agent.

The use of liposomes for the delivery of imaging agents has quite a long history. The ability of liposomes to trap different substances in both the aqueous phase and the liposome membrane compartment makes them suitable for carrying diagnostic moieties used with many imaging modalities. Differences in the chemical nature of the reporter moieties used in different modalities require a range of protocols for loading liposomes with the given contrast agent. Furthermore, imaging modalities differ in sensitivity and resolution and may require different amounts of a diagnostic label to be delivered to the area of interest. These general considerations have led to the development of a family of liposomal contrast agents for various purposes. Computed tomography contrast agents are included primarily in the inner water compartment of liposomes or incorporated into the liposome membrane. Liposomes for ultrasonography are prepared by incorporating gas bubbles, which are efficient reflectors of sound, into the liposome or by forming a bubble directly inside the liposome as a result of a chemical reaction such as bicarbonate hydrolysis, yielding carbon dioxide

[Unger et al. 1994; Matteucci & Thrall 2000]. Gamma-scintigraphy and MRI both require that a sufficient quantity of radionuclide or paramagnetic metal be associated with the liposome. Metals can be incorporated into an appropriate chelating compound (for example, diethylene triamine pentaacetic acid, DTPA) and then introduced into the aqueous interior of a liposome. Various chelators and hydrophobic anchors have been used successfully for the preparation of liposomes containing indium (In), metastable technetium (Tc), manganese (Mn) and gadolinium (Gd) [Matteucci & Thrall 2000]. MRI using contrast liposomes is quite well advanced. Normally, liposomal contrast agents act by shortening the relaxation times (T1 and T2) of water protons in the surrounding aqueous environment, resulting in an increase (T1 agents) or decrease (T2 agents) in the intensity of the tissue signal. For an optimal signal, all the reporter metal atoms should be freely exposed to interaction with water molecules. This requirement makes metal-ion encapsulation into the liposome less attractive than metal-ion coupling with polymeric chelators exposed to the outer water space. Mn and Gd, which provide sufficient changes in relaxation times, are usually used to prepare liposomal contrast agents for MRI [Torchilin 1996]. Two principal approaches to improve Gd-containing liposomes as magnetic resonance (MR) contrast media for the visualisation of lymph nodes have been suggested: (1) increasing the quantity of liposome-associated Gd by using membrane-anchored chelating polymers; and (2) enhancing signal intensity by modifying Gd-liposomes with certain polymers. In principle, liposome modification with Gd-DTPA-polylysine-based chelating polymer increases the metal load per vesicle severalfold, while surface modification with PEG leads to increased relaxivity (better signal at the same tissue concentration) of paramagnetic vesicles. Coating liposomes of this type with PEG may change the aqueous environment of the Gd metal because water molecules associate tightly with the PEG molecules, resulting in an increase of signal over 'noise'. Using this method, regional lymph nodes in rabbits were visualised within minutes of subcutaneous injection of PEG-modified Gd-containing liposomes or liposomes modified with Gd-loaded polychelate. The combination of the particulate nature of liposomes with the increased MR signal from PEG-liposome-bound Gd ions is a major advantage of the liposomal MRI agents compared with conventional soluble Gd derivatives, which accumulate slowly in lymph nodes (Torchilin 1996).

Technically, it should be possible to detect the distribution of nanoparticles within the inner ear *in vivo* with MRI if the nanoparticles contain paramagnetic agents such as gadolinium chelate. The disadvantage

of using chelated Gd is that the amount of Gd must be relatively high to be visualised; therefore, a significant part of the carrier capacity of nanoparticles must be reserved for Gd.

Treatment of inner ear diseases remains a problem because of limited passage of drugs through the blood-inner ear barrier and lack of control over the delivery of treatment agents by intravenous or oral administration. As a minimally invasive approach, intratympanic delivery of multifunctional liposomes carrying genes or drugs to the inner ear is a potential future method for treating inner ear diseases, including sensorineural hearing loss and Ménière's disease. In designing such an approach, it is important to track the dynamics and distribution of liposomes *in vivo*. In particular, in the process of optimising the functionalisation of each type of liposome, it is essential to be able to trace its passage through the cochlea. However, tracking the passage of multifunctional liposomes through the inner ear by histological means is problematic. First, autofluorescence from lipofuscin granules, which are found in the cochleae of humans, chinchillas, guinea pigs and rats, impairs the detection of fluorescent signals from the multifunctional liposome targets [Ishii 1977; Bohne et al. 1990; Igarashi and Ishii 1990; Horner and Guilhaume 1995; Walther and Westhofen 2007; Zhang et al. 2010]. Second, the inner ear is composed of fluids, soft tissue, and bone (Figure 5.9). This results in signal loss in histological study, which is incapable of retaining the inner ear fluids. Finally, it is inconvenient to observe the dynamics of multifunctional liposomes in the inner ear in histological studies. MRI techniques, on the other hand, have made it possible to examine the compartments of the cochlea using nanoparticles labelled with a contrast agent. Gadolinium-tetra-azacyclo-dodecane-tetra-acetic acid (Gd-DOTA) was shown to be efficiently taken up into rat inner ears and detected at 60 min post-transtympanic injection, with greater signal intensity observed in the scala vestibuli than in the scala tympani and no uptake into the endolymph after 4 h [Zou et al. 2010]. Gd-DOTA is known to be clinically safe and has great diagnostic value (Herborn et al. 2007). Encapsulation of Gd-DOTA into the liposomes is necessary because this increases the amount of gadolinium available for MR imaging. MRI-traceable liposomes can be further developed as multifunctional nanoparticles. The use of MRI to track the dynamics and distribution of liposomes in the inner ear *in vivo* allows investigators to predict the destination of these liposomes when they are used clinically to carry genes or drugs.

3. Aims of the Study

The overall aim of this study was to developing multifunctional liposomes that can deliver drugs or genes with peptide-driven targetability and that can be visualized by MRI, using the inner ear as a model target organ. This work has potential applicability to the development of therapies for disorders of the inner ear.

1. As the first aim, the main effort was to prepare liposomes with a diameter less than 100 nm, avoiding loss of material observed in extrusion.

2. The second aim of this study was to make liposomes containing the neurotoxic drug disulfiram to analyse the efficacy of their penetration through the RWM when injected into the middle ear cavity of mice and to determine whether the amount of liposomes accumulating in the inner ear tissues was sufficient to elicit biological effects in the inner ear.

3. Under the third aim, this study investigated the selective targeting of liposomes to TrkB-expressing cells using peptide-conjugated liposomes (PCL). TrkB suppressive targeting is considered relevant in therapies for neuroblastoma and other tumors and its activation is thought to play a beneficial role in neuronal survival.

4. Our fourth aim was to develop MRI-traceable liposomes by encapsulating gadolinium and to use these liposomes to track the dynamics and distribution of liposomes in the rat's inner ear.

4. Materials and Methods

4.1 Materials

DPPC, LysoPC, and POPG, were from Lipoid GmbH (Ludwigshafen, Germany). Chol, EggPC, DMPE-DTPA (Gd), DOPE, DPPG, DSPE-PEG-2000, DSPE-PEG (2000) maleimide, NBD-PC, SOPC, Sph, were from Avanti Polar Lipids (Alabaster, AL). Dichloromethane, disulfiram, EDTA, and Hepes were from Sigma-Aldrich (St Louis, MO). Gd-DOTA (DOTAREM) was from Guerbet, Cedex, France. Polycarbonate membrane filters were purchased from Millipore, Bedford MA. HPLC-grade TFA was from Fluka (Buchs, Switzerland) and acetonitrile from Rathburn (Walker Burn, Scotland, UK). TRITC-DHPE (II) or DPPRho (III) was from Molecular Probes (Eugene, OR, USA). The purity of lipids was checked by thin layer chromatography on silicic acid coated plates (Merck, Darmstadt, Germany) developed with a chloroform/methanol/water mixture (65:25:4, v/v/v). Visual examination of the plates after iodine staining or upon UV illumination revealed no impurities. Lipid concentrations were determined gravimetrically with a high precision microbalance (either with SuperG, Kibron, Espoo, Finland or with Cahn, Cerritos, CA, USA). The concentration of fluorescent lipids were determined spectrophotometrically using a molar absorptivity ε_{465} = 19000 $M^{-1}cm^{-1}$ (in C_2H_5OH). Other chemicals were of analytical grade and from standard sources. Unless otherwise indicated all experiments were conducted in 20 mM Hepes, 0.1 mM EDTA, and pH 7.4, at 25 ^{o}C.

Other materials

Other materials used in the study were described in respective original publications (I, II, III, and IV).

4.2 TrkB-binding peptides (III)

TrkB binding peptides were designed based on published TrkB-binding sequences (see Table 5.1 at page no. 57).

In brief, peptides A366, A367, A368, A369 and A370 were described by Ma et al. [2003], except for covalently coupled fluorescein. The above peptides were synthesized from the C-terminus while coupled via a hydrazine bridge to an activated resin (Storkbio, Tallinn, Estonia). After cleavage and before deprotection of the NHS ester, the peptides were reacted with FITC. A371, corresponding to the neurotrophin sequence 84-100 TFVKALTMDGKQAAWR, which has been shown to bind to TrkB. Scr-A371, with the same amino acid composition as A371, but in a random order. A415, containing the TrkB binding sequence of A366, with a Tobacco Etch Virus (TeV) protease cleavage site (CENLYFQSG, cleavage between Q and S) added to the N-terminus. Scr-A415, a scrambled version of A415 with the TrkB binding motive in a random order and A417, the retro-inverse version of A415 with the binding motive composed of D-amino acids in a reverse order.

4.3 Experimental animals (II, IV)

Details concerning the experimental animals used in this study are given in the respective publications (II, IV)

4.4 Focused ultrasound (I)

MLV with different lipid compositions were subjected to acoustic energy using AFU sonicator (S2, Covaris, Inc., Woburn, MA) under conditions described in detail in Results and Discussions section of this thesis.

4.5 Dynamic light scattering (I, II, III, IV,)

Average hydrodynamic particle diameter (Z_{av}) and polydispersity index (PDI) of lipid vesicles were determined by dynamic light scattering (DLS) at 25 °C (Zetasizer Nano ZS, Malvern Instruments Ltd., U.K.). The instrument employs photon correlation spectroscopy to characterize the dynamics of the particles on the basis of a Brownian motion model, [Koppel 1972] collecting backscattering at an angle of 173°. By cumulant analysis of the measured intensity autocorrelation function, PDI was obtained as the relative variance of the average diffusion coefficient, *D*. Z_{av} was inferred from *D*, using the Stokes–Einstein relation, which for spherical particles

takes the form $Z_{av} = kT/3\pi\eta D$, where k is the Boltzmann constant, T is the absolute temperature, and η is the shear viscosity of the solvent. In all DLS measurements, each data point represents the mean of three independent measurements.

4.6 Differential scanning calorimetry (I)

Liposomes were loaded into the calorimeter cuvette before and after AFU treatment (final concentration of 1 mM). A microcalorimeter (VP-DSC, Microcal Inc., Northampton, MA) was operated at a heating rate of 0.5 degrees/min. All scans were repeated to assure reproducibility. Deviation from the baseline was taken as the beginning of the transition and return to the baseline as its end. The instrument was interfaced to a PC, and the endotherms were analyzed using the routines of the software provided by the instrument manufacturer.

4.7 Dithionite assay (I)

To confirm the lamellarity of the liposomes, the dithionite quenching assay was employed [McIntyre and Sleight 1991]. For this assay, a fluorescent phospholipid analog NBD-PC (X = 0.01), was incorporated into the vesicles (100 μM total lipid concentration). NBD can be reduced by dithionite to the non-fluorescent product 7-amino-2, 1, 3-benzoxadiazol-4-yl, permitting the assessment of the amount of this probe in the outer leaflet of the bilayer. The fluorescence intensity of the lipid solution was recorded before and after the addition of an aliquot of a freshly prepared, ice-cold, 50mM dithionite solution in 20 mM Hepes, 0.1 mM EDTA, pH 7.4 using a Perkin Elmer LS 50B spectrofluorometer (Wellesley, MA) interfaced to a computer, with 4 nm band passes and excitation and emission wavelengths of 470 and 540 nm, respectively. The intensity values for stable fluorescence readouts were used to calculate the percentage of quenching of NBD fluorescence. Cuvette temperature was maintained at 25 °C with a circulating water bath, and the contents of the cuvette were mixed using a by a magnetic stir bar. Unilamellarity is assumed when ~ 50 % quenching is measured upon the addition of dithionite. The initial rapid decline in the emission intensity was followed by a very slow fluorescence loss due to flip-flop of the NBD probe from the inner leaflet.

4.8 Cryogenic transmission electron microscopy (I)

The vitrified samples of vesicles generated by AFU were prepared on Protochips C-Flat 224 grids as previously described [Baker et al. 1999]. A Gatan 626 cryostage was used to observe the sample in a FEI Tecnai F20 field emission gun transmission electron microscope at 200 kV under low-dose conditions and −180 °C. The images were recorded using a Gatan Ultrascan 4000 CCD camera at a nominal magnification of 68000×.

4.9 Stability of liposomes (I, II, III, IV,)

Liposome stability is a key parameter controlling the shelflife of the preparations. To check the stability of the lipid vesicles they were stored at 4 °C for several days and changes in their size distributions upon ageing were assessed by DLS.

4.10 Preparation of lipoplexes

After being subjected to focused ultrasound, liposomes were mixed with plasmid DNA at a lipid/DNA charge ratio (+/-) of 1.2:1 to obtain nanoscale particles (also termed nanoplexes). The final concentration of lipids in lipoplexes was 0.1 mM. After the addition of pDNA, the Z_{av} and polydispersity of liposomes were obtained using DLS.

4.11 Confocal microscopy (II, III)

Fluorescence signals of rhodamine from liposomes (excitation 540 nm) were detected using a confocal microscope (Zeiss 510 DUO) with the appropriate band pass and long pass emission filters. Frame sizes were from 1024 × 1024 up to 2048 × 2048 pixels and the colour depth was from 8 to 12 bit. Z stacks through the SG were acquired for stereological analysis.

Localization and binding of the designed peptides were assessed by employing a Zeiss LSM-510 META confocal microscope using a 63x, 1.4 NA (oil) plan apochromate lens. Samples were illumination at 488 nm (R-phycoerythrin) and 633 nm (Alexa Fluor 633) lasers and detection at 520 nm with a bandpass filter and at 650 nm with a longpass filter, respectively.

4.12 Magnetic resonance imaging (IV)

A 4.7 T MR scanner with bore diameter of 155 mm (PharmaScan, Bruker BioSpin, Germany) was used in both phantom and *in vivo* MR measurements. The maximum gradient strength was 300 mT/m with an 80-µs rise time. A dedicated rodent head coil (linear bird cage coil) with diameter of 38 mm was used for the phantom and animal studies.

4.13 Other methods

All other methods used in this study are as described in respective original publications (I, II, III, and IV).

5. Results and Discussion

5.1 Making unilamellar liposomes using focused ultrasound

Several techniques are available for making LUV with an average diameter of approximately 100 nm. These liposomes are widely employed as model biomembranes as well as vehicles for drug delivery. LUV provide a number of advantages as drug carriers, including efficient encapsulation of water-soluble and insoluble drugs, economy of lipid consumption, and reproducible drug release rates. We have used the instrument AFU to down-size MLV into LUV (Figure 5.1). The instrument employed by us works with a centre frequency of approximately 500 kHz, corresponding to a wavelength of a pproximately 2 mm. The main parameters controlling the acoustic signal that can be adjusted in this equipment are:

Duty cycle (DC): Percentage of the time, during one *On*/*Off* transducer cycle, where the transducer is "On", emitting acoustic energy. The instrument used has a maximum DC of 20%.

Cycles per burst (CPB): Number of pressure waves contained in the wavetrain produced during each "On" period in the transducer. In AFU at ultrasound frequency *f*, this parameter controls the duration of the "On" periods in the transducer, T_{On} = CPB/*f*, and also determines the length of the *Off* period as follows:

$$T_{Off} = \frac{CPB}{f}\left(\frac{100}{DC} - 1\right) \qquad \textit{equation 1}$$

Intensity: The amplitude of the acoustic pressure waves produced by the transducer into the solvent phase. In the instrument employed the intensity values can be varied between 0 and 10 on an arbitrary scale.

Treatment time (t): The duration of the sonication procedure, which has been shown to be an important parameter that can be correlated with a decrease in the mean size and polydispersity of the final dispersion of vesicles [Woodbury et al. 2006]

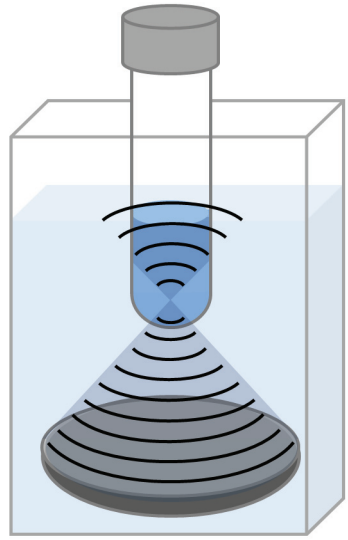

Figure 5.1: Schematic illustration of the AFU acoustic field during an ON period in the transducer, showing the focus of the ultrasound emitting from the concave surface of the transducer. Both the transducer and the sample are contained in a thermostatted water bath.

The significance of DC and CPB is illustrated by the schematic examples depicted in Figure 5.2. Apart of these sonication parameters, the vesicle characteristics are influenced by factors such as lipid concentration, temperature, and sample volume, as well as by the properties of the lipids used, such as:

Charge: This is directly related to the membrane properties of the formed vesicles, affecting their size, and the final colloidal stability.
Lipid packing: The phase state and organization of the saturated or unsaturated lipids in the membrane can be readily expected to influence the average vesicle size and system thermodynamic stability. Packing is in part controlled by the effective shapes of the lipids [Thuren 1986; Janmey and Kinnunen 2006] for two or more lipid components, the molar ratio also being a key parameter to be considered.
Dispersant characteristics: The characteristic of the solvent phase such as its density, viscosity, and surface tension are directly related to the impact of the propagating energy on the MLV.

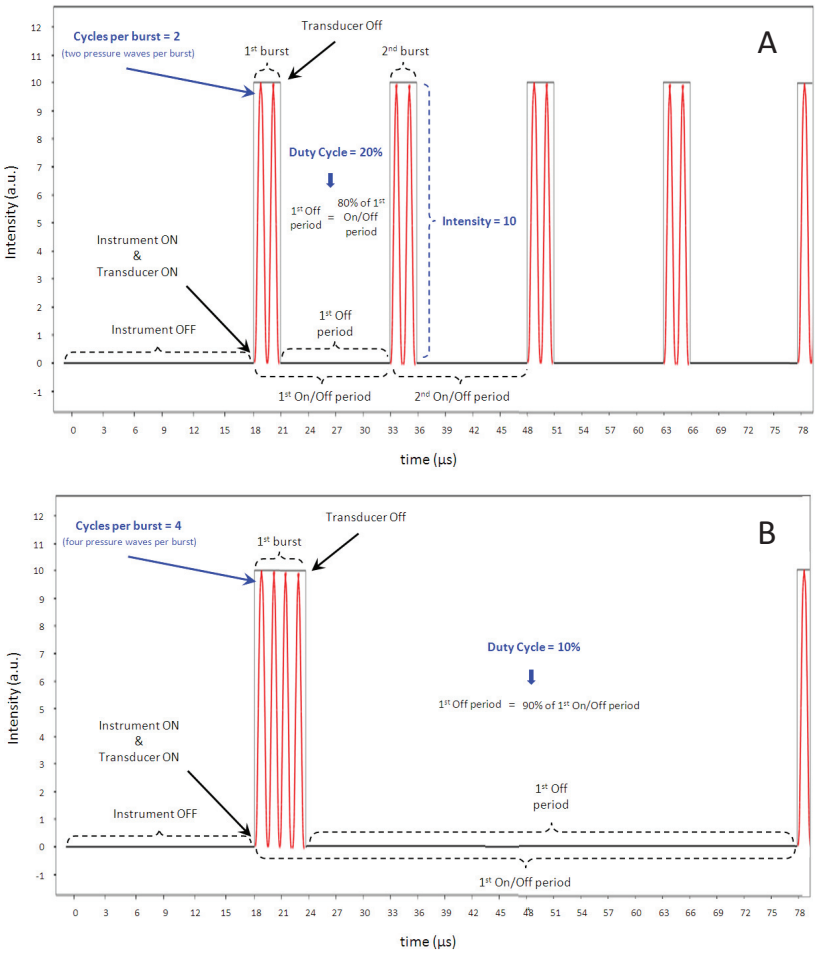

Figure 5.2: Schematic illustration of the AFU transducer output employing (**A**) intensity 10, 2 CPB with 20 % DC, and (**B**) intensity 10, 4 CPB with 10 % DC.

As there was essentially no prior art in the use of AFU for obtaining LUV, we had to establish initial conditions by trial and error. Using different lipid compositions, the parameters investigated in our first preliminary trials were those controlling the output of the AFU; in these trials, we recorded the impact on liposome size distribution by DLS. We could quickly abandon the use of low duty cycles because these showed no clear effects on the size distribution when the other parameters were varied. We then focused on the impact of intensity and CPB on the formation of vesicles composed of DPPC or SOPC and treated for 20 min. As mentioned above, CPB controls the length of the transducer *On/Off* periods, thus modulating the duration of the pressure wavetrains and the relaxation times between them. Depending on the total treatment time and lipid composition, the results

revealed optimum values for the duration of the transducer *On/Off* periods, for obtaining LUV with $Z_{av} \approx 100$ nm.

Initial experiments revealed that intensity settings below 8 did not produce vesicles with average diameters smaller than 500 nm (data not shown). This could be due to (*a*) the inability of these energies to disrupt MLV into phospholipid bilayer fragments (PBF) or (*b*) to the formation of large PBF unable to form small liposomes. At higher intensities downsizing of MLV into smaller vesicles could be observed. For DPPC there was a clear difference in the sizes of vesicles produced at intensity settings 8 and 10. At intensity 8 the particles were larger than those obtained at intensity 10 but had similar PDI (Figure 5.3). In contrast, for SOPC both Z_{av} and PDI were similar at these intensities (Figure 5.3). This result likely to reflects the different phase states of these two phospholipids at the treatment temperature, 25 °C; at this temperature, DPPC is below its T_m, and SOPC is in the liquid disordered (fluid) phase. For solid ordered DPPC, higher intensities may give rise to smaller PBF that then assemble into smaller vesicles. As intensity decreases, the dynamics of formation of cavitation bubbles change [Brennen 1995] producing microstreaming of different strengths. Due to higher membrane elasticity, for lipids such as SOPC (above T_m), the formation of similar PBF is likely also to be achieved with lower microstreaming energies.

Some values of CPB were observed to produce monodisperse DPPC and SOPC vesicles with $Z_{av} \approx 100$ nm (Figure 5.3). Under these conditions, it is likely the presence of stable cavitation bubbles causing microstreaming and creating shear enough to produce smaller PBF [Richardson 2007]. When maintaining constant values for DC, the value of CPB controls the length of the transducer *On/Off* periods (eq. 1). Three effects by CPB can be considered (Figure 5.3):

i) Low CPB values may not transmit enough acoustic energy to cause the formation of PBF and a simple excision of polydisperse large vesicles from the MLV may take place.

ii) At high enough CPB, PBF are generated with subsequent fusion into small vesicles during long enough transducer *Off* periods. In our experiments optimum values for CPB yielding $Z_{av} \approx 100$ nm were observed between 100 and 500 CPB.

iii) High CPB values increase the duration of the transducer *On* periods which could decrease the size of the formed PBF. Accordingly, at constant DC the corresponding longer *Off* periods upon increasing CBP may allow PBF assemble into a

more polydisperse collection of larger vesicles, as observed (Figure 5.3).

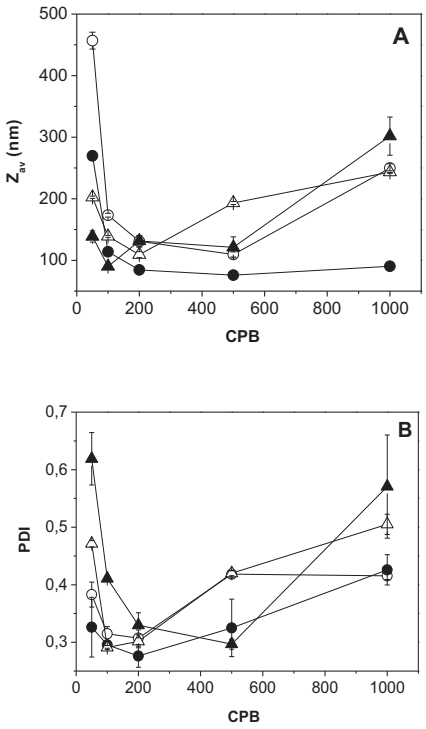

Figure 5.3: Dependence of Z_{av} (**A**) and PDI (**B**) on CPB during 20 min AFU at 25 ºC of 5 ml samples of 0.1 mM DPPC MLV at intensity 8 (○) or 10 (●), and 0.1 mM SOPC MLV at intensity 8 (Δ) or 10 (▲).

Our results demonstrate that by varying the intensity and CPB, depending on the saturation of the lipid acyl chains, it is possible to modulate the size of the vesicles and to diminish their polydispersity. The presence of unsaturated acyl chain eliminates differences between size distributions obtained at intensity settings 8 and 10 and has no effect on the trends observed for different CPB. The dithionite assay revealed that the vesicles obtained in this way were largely unilamellar.

Binary liposomes

In order to evaluate the influence of surface charge on the formation of LUV by AFU, we prepared MLV composed of DPPG and DPPC at different molar ratios, viz. 0.05:0.94, 0.2:0.79, 0.4:0.59 and 0.99:0.00. NBD-PC (X = 0.01)

was additionally included to allow to assess the lamellarity of the liposomes. MLV were treated for 20 min at intensity 8 or 10, varying CPB. No differences in Z_{av} and PDI were evident upon changing CPB or lipid composition (Figure 5.4, *A-D*). Accordingly, increase in the negative surface charge due to the inclusion of DPPG is without effect.

Saad et al. [2009] demonstrated that increasing the content of DPPG in a mixture with DPPC up to 50% does not change the elasticity of mixed monolayers. In order to vary the membrane elasticity of liposomes, we repeated the above experiment using the unsaturated POPG instead of DPPG. POPG/DPPC MLV were made at molar ratios of 0.05:0.94, 0.2:0.79, 0.4:0.59 and 0.99:0.00. Pronounced impact on Z_{av} and PDI by CPB and the lipid stoichiometry could now be observed (Figure 5.4, *E-H*). Importantly, the same values of CPB yielding for zwitterionic lipids low PDI now yielded large aggregates with high polydispersity. At the two intensities applied, 8 and 10, and for CPB close to 200, both Z_{av} and PDI increased with $X_{POPG} > 0.2$. This inversion in the change of Z_{av} and PDI with respect to CPB for vesicles containing POPG indicates a possible synergetic effect of increasing surface charge and increasing membrane elasticity due to the unsaturated acyl chain. Because of latter, a more loose packing and increased membrane elasticity and less resistance to stretching and bending is expected.

For the zwitterionic liposomes, the optimum values of CPB (~200) for obtaining LUV with low PDI are likely to reflect the formation of properly sized PBF fusing and assembling during sufficiently long relaxation periods. For liposomes containing POPG, these same AFU parameters result in the formation of larger and more polydisperse PBF, able to fuse and assemble into a highly polydisperse collection of vesicles. The different durations of the transducer *On/Off* periods, above or below 200 CPB, may produce either monodisperse, smaller PBF with longer *Off* assembling times or the excision of smaller PBF from MLV at lower CPB. This is consistent with the formation of SUV (Z_{av} = 50 ± 5 nm, PDI = 0.20 ± 0.05) at CPB above 400, with a minimum in PDI for POPG:DPPC (0.2:0.8, molar ratio) in all cases. Higher contents of DPPC yield again smaller diameters and less polydispersity, as seen for neat DPPC at 200 CPB.

At intensity 10, both Z_{av} and PDI changed with CPB and lipid composition similarly as when using intensity 8. These changes occurred in a narrow range of CPB and lipid ratios, appearing at X_{POPG} above 0.5 and at CPB between 50 and 400 (Figure 5.4, *G-H*). Higher ultrasound energy seems to yield less polydisperse PBF, with a smaller change in liposome size depending on the elasticity of the lipid compositions and the relaxation times of AFU.

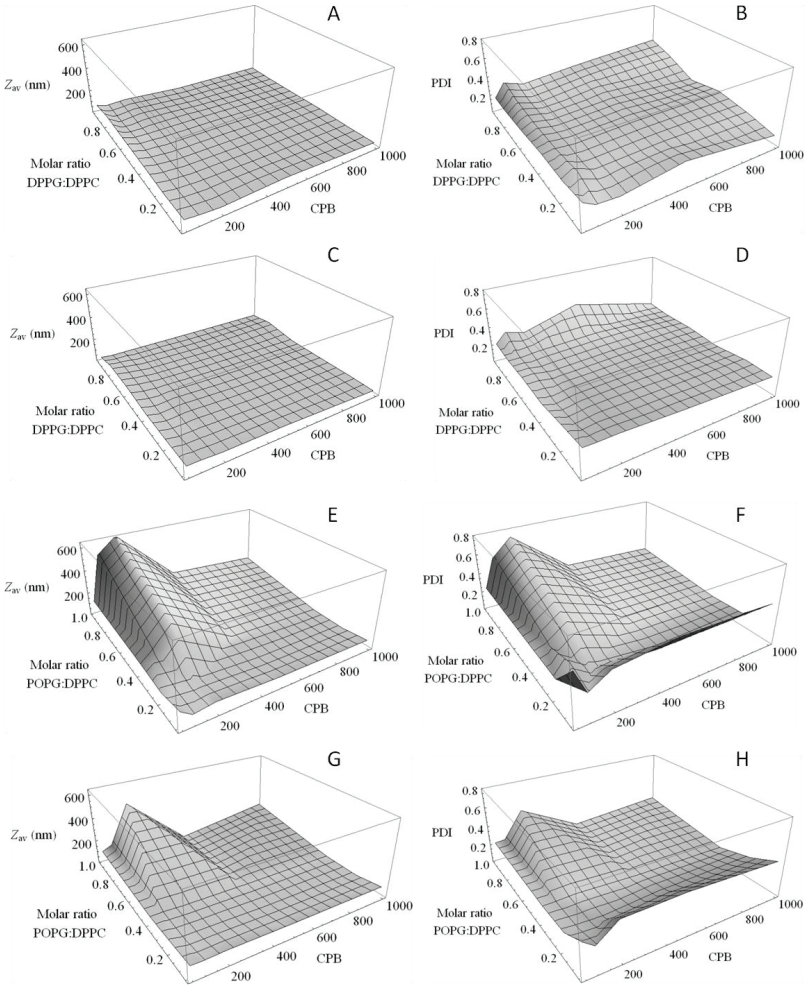

Figure 5.4: Dependence of Z_{av} and PDI on AFU CPB and on the molar ratio of the constituent phospholipids in 0.1 mM DPPG:DPPC MLV at intensity 8 (**A**, **B**) and at intensity 10 (**C**, **D**). Similar data but for POPG/DPPC at intensity 8 (**E**, **F**) and at intensity 10 (**G**, **H**). Samples were in 5 mL of buffer. Total time for sonication was 20 min at 25 °C. All liposomes additionally contained NBD-PC (X = 0.01).

Effect of AFU treatment time

In general, longer AFU treatment decreased Z_{av} irrespective of the other parameters used. For SOPC Z_{av} decreased upon prolonging the sonication time while values for PDI remained unaltered (Figure 5.5). This was evident also for compositions forming more rigid membranes, such as POPG:DPPC:Chol (65:5:30, molar ratio) and POPG:DPPC:Chol (50:20:30, molar ratio), for which Z_{av} decreased, whereas PDI was unaffected. For

these compositions, cholesterol may well be responsible for the lack of changes in PDI. Differences in acyl chain saturation, treatment intensity, or CPB do not seem to affect the above findings (Figure 5.5).

DPPC: Chol: DSPE-PEG-2000 (75:20:5, molar ratio) corresponds to the liposome formulation Doxil® developed for anticancer drug delivery [Lasic 1996]. This composition involves high membrane rigidity due to the presence of cholesterol and saturated lipids. For this lipid mixture constant values of Z_{av} and decrease in PDI for a 20 min treatment were evident (Figure 5.5). We can conclude that the relation between longer treatment time and reduced vesicle size does not hold for all lipid compositions and depends on the parameters describing lipid packing and on the stability of PBF and the assembling vesicles.

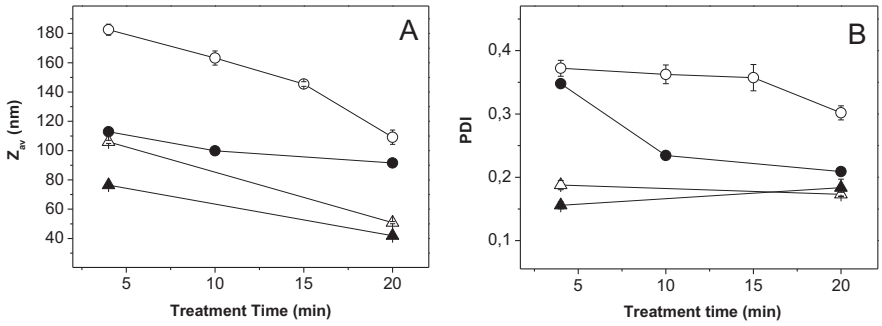

Figure 5.5: Dependence of the Z_{av} and PDI (**A**, **B**) on the AFU treatment time, varied from 4 to 20 min. The samples (5 ml of 100 μM total lipid) were SOPC, sonicated at intensity 10 and CPB 200 (○), DPPC:Chol:DSPE-PEG-2000 (75:20:5, molar ratio), treated at intensity 8 and CPB 200 (●), POPG:DPPC:Chol (65:5:30, molar ratio) at intensity 10 and CPB 100 (Δ), and POPG:DPPC:Chol (50:20:30, molar ratio) at intensity 8 and CPB 500 (▲). Temperature was maintained at 25 °C.

5.1.1 Differential scanning calorimetry

The commonly employed membrane models MLV and LUV differ significantly in their thermal phase behavior [Parry 2010]. Proper understanding of the physicochemical properties of LUV obtained by AFU is essential for their possible use as model membranes or as drug or gene delivery vehicles. Differential scanning calorimetry (DSC) was used to check the differences in the thermal phase behavior of DPPC MLV and LUV prepared by AFU (Figure 5.6). Even when the total enthalpy for the AFU LUV is more or less the same as for MLV, LUV made by AFU revealed a broader asymmetric endotherm than MLV, peaking at 41 °C, corresponding

to the main phase transition temperature. The lowermelting component could be due to the presence of PBF in the samples. MLV exhibit two well discernible endothermic phase transitions at 35.3 and at 41.3 °C, corresponding to the pretransition between the gel (L_β) and rippled (P_β) phases, and to the main (chain melting) transition between the rippled and liquid crystalline (L_α) phases, respectively. The pretransition is weak for pure DPPC LUV, and it has been suggested that the formation of the P_β phase by MLV requires interlamellar coupling, which is absent for the separated bilayers in LUV [Parry 2010]

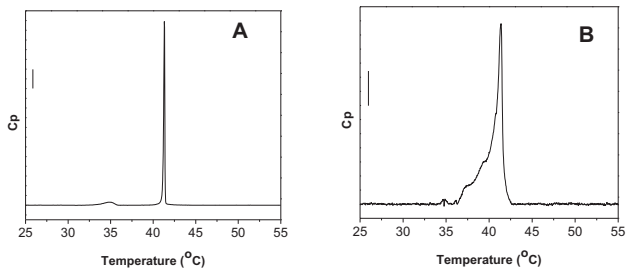

Figure 5.6: Heat capacity scans (Cp) for (**A**) 1 mM DPPC MLV and (**B**) AFU LUV. The calibration bars correspond to 2 and 1 kJ/deg mol^{-1} in (**A**) and (**B**), respectively.

5.1.2 Cryo-TEM

Vesicles generated by AFU were analyzed also by cryogenic transmission electron microscopy (cryo-TEM). DPPC MLV (0.1 mM) treated during 20 min at 20 DC, intensity 8, and 100 CPB (Figure 5.7A) were unilamellar and showed sizes on the range of those obtained by extrusion of 1 mM MLV through 200 nm pore polycarbonate filters (Figure 5.7B). Their Z_{av} was slightly above 100 nm and they exhibited a dimpled surface compared to the smooth appearance of the extruded liposomes. Accordingly, the AFU-generated LUV are likely to be tension free. Micrographs consistently revealed PBF (Figure 5.7A, white arrows). When a higher (20 mM) concentration of DPPC/LysoPC/DSPE-PEG-2000 (87:9:4, molar ratio) MLV was sonicated by AFU using the former parameters, the number of PBF increased. LysoPC may stabilize the contour of these PBF while the PEG conjugate reduce their assembly rate. In this way it was possible to observe more PBF after the AFU treatment and also to analyze their mechanism of assembly into unilamellar vesicles (Figure 5.7, C-F). Possible fusion of two PBF is likely to be taking place in Figure 5.7C (white arrow). Self-closure of bigger membrane fragments produced by PBF fusion was

occasionally seen (Figure 5.7D, white arrows). Below this self-closing vesicle there is an already formed LUV. PBF trapped inside a LUV during the vesicle closure was also captured (Figure 5.7E, white arrow), with possible selfassembly when two or more PBF were trapped in this way Figure 5.7F (white arrow). The phospholipid bilayer fragments illustrated in the Cryo-TEM photographs (Figure 5.7, D-F) were consistently seen for a large number of samples analyzed. These cryo-TEM micrographs corroborate the mechanism for formation of unilamellar vesicles by sonication after the disruption of MLV into PBF and their subsequent fusion and self-assembly into LUV [Lasic 1987].

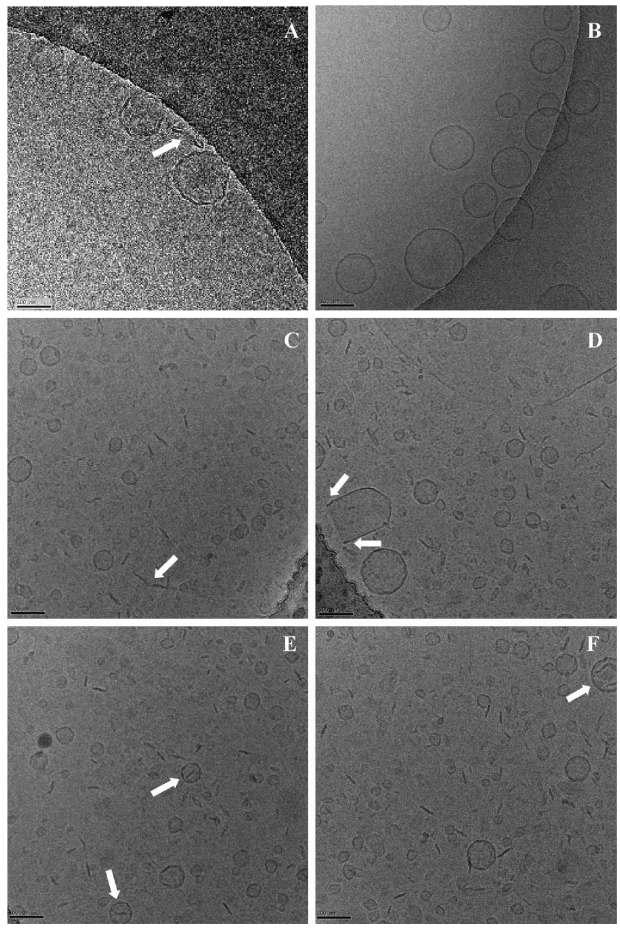

Figure 5.7: Cryo-TEM images of (**A**) 0.1 mM DPPC MLV after 20 min AFU at intensity 8, DC 20 and CPB 100; (**B**) 1 mMDPPC MLV passed through polycarbonate filters of 200 nm pore; (**C**-**F**) 20 mM DPPC/LysoPC/DSPE-PEG-2000 (87:9:4, molar ratio) MLV after 20 min AFU at intensity 8, DC 20 and CPB 100.

5.1.3 Stability

Liposome stability is a key parameter controlling the shelflife of the preparations. To check the stability of lipid vesicles prepared using AFU, they were stored at 4 °C for several days and changes in their size distributions upon aging were assessed by DLS. For the Doxil formulation, we observed an increase in the mean size and polydispersity with time. This was particularly clear during the first two days of storage. As in the former experiments, it was again possible to observe optimum CPB values corresponding to minimum mean sizes (100 nm). Interestingly, these optimum values (500 CPB) did not influence the PDI values, which increased linearly with CPB. These results may relate to the steric stabilization imparted by the PEGylated lipid upon the formation and assembly of PBF, together with the enhanced stability of the vesicles formed.

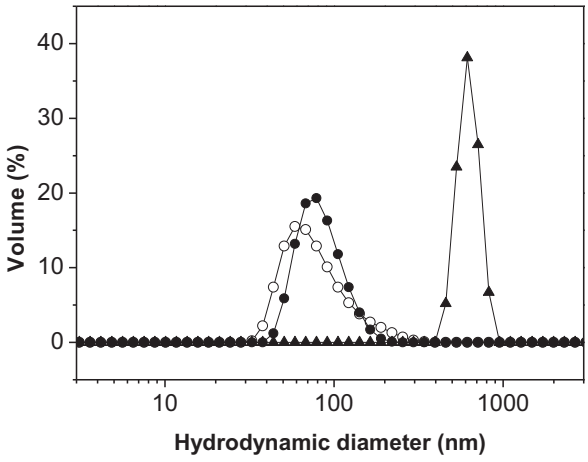

Figure 5.8: Size distributions (vol %) for 100 µM DPPC MLV after lipid film hydration (▲), after extrusion through 100 nm polycarbonate filter (●), and after 20 min AFU at 25ºC (○, intensity 8, CPB 100).

In conclusion, for most lipid compositions we were able to establish a combination of AFU parameters yielding monodisperse unilamellar vesicles with $Z_{av} \approx 100$ nm (Figure 5.8).

5.2 Cochlear targeting of disulfiram-loaded liposomes after application to the RWM in mouse

The World Health Organization has estimated that 278 million people worldwide suffer from moderate to profound hearing loss in both ears, making hearing loss one of the most prevalent chronic conditions worldwide [WHO 2012]. The EU has ranked hearing impairment in the seventh place on the disability list, with more than 60 million citizens affected by hearing loss at an annual cost of 107 billion euros [WHO 2008]. The inner ear is a highly organised, relatively immunoprivileged, isolated sensory organ localised in the bony cochlea. The RWM is permeable to small molecules and can be used as an access route to the inner ear.

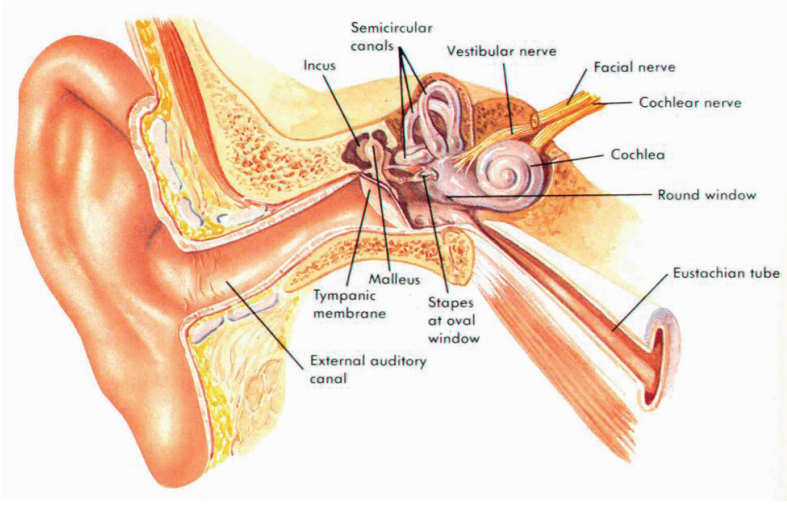

Figure 5.9: Gross anatomy of the ear-frontal section. (Reprinted with permission from Dr. Janos Madar from http://jmbodycare.blogspot.com/p/hopi-ear-candles.html).

Direct drug delivery to the cochlea is associated with the risk of irreversible damage to the ear, which may lead to permanent alteration of both hearing and balance. We have used liposome nanoparticles as potential tools for drug delivery to the cochlea through application to the RWM in mice. The transport of liposomes (marked with rhodamine) from the middle ear to the cochlea was investigated using unloaded or loaded with disulfiram as a toxicity model drug.

5.2.1 Disulfiram-loaded liposomes

Liposomes containing disulfiram were prepared by reversed-phase evaporation with minor modifications [Szoka and Papahadjopoulos 1978]. Appropriate amounts of lipid stock solutions were transferred into glass test tubes. The lipid/drug molar ratio was 0.85:0.15 (eggPC: DSPE-PEG-2000: TRITC-DHPE: disulfiram = 0.77:0.05:0.03:0.15). The solvent was removed under a stream of nitrogen, and the dry residue was subsequently maintained under reduced pressure overnight. The lipid film was dissolved in dichloromethane; this solution was used as the hydrophobic phase. The dichloromethane solution was mixed with buffer (10 mL, 5mM Hepes, 0.1mM EDTA, pH 7.0) and the suspension subsequently treated for 100 seconds using AFU at instrument settings of DC 20, intensity 10, and 500 CPB. The samples were Subsequently maintained at 37 °C for 10 min to remove the solvent. The resulting dispersion was then passed through an extruder with polycarbonate membrane filters of 100 nm pore size. The final lipid concentration in the sample was 1 mmol. The lipid:disulfiram loading ratio was one molecule of disulfiram to five molecules of phosphatidylcholine.

The highly lipophilic nature and poor water solubility of disulfiram promotes its sequestration into the liposomes, where it intercalates into the hydrocarbon region of the phospholipids. This was calculated stoichiometrically to be 150 μmol. The liposomes contained a rhodamine conjugated lipid (TRITC-DHPE) as a traceable fluorescent marker for *in vivo* studies. The average size of the liposome nanoparticles used was 82 ± 5 nm with a PDI = 0.05 (Figure 5.10).

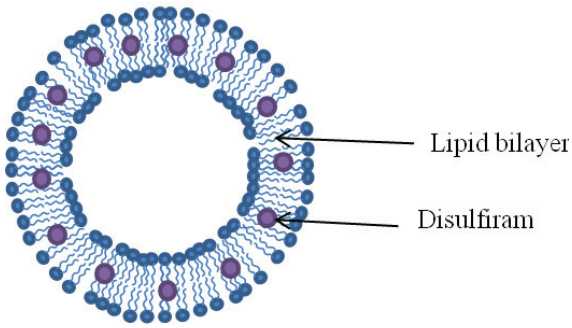

Figure 5.10: Schematic representation of a disulfiram-loaded liposome.

5.2.2 Effects of disulfiram-loaded liposomes

5.2.2.1 Morphological changes in the cochlea after application of disulfiram-loaded liposomes

To determine whether the amount of disulfiram-loaded liposomes that reach the cochlea is sufficient to elicit a functional effect, they were applied to the RWM of mice. Animals were sacrificed 2, 7 and 14 days after injection of liposomes loaded with disulfiram. The distribution of the disulfiram-loaded liposomes at these times was similar to that of the unloaded liposomes, particularly in the SG. Disulfiram released from the liposomes produced significant damage to both neurons and Schwann cells in the SG as indicated by Nissl, S100, active caspase 3, and Fluorojade staining. Sections stained with cresyl violet displayed random loss of SG neurons in the basal and middle cochlear turns. The loss of SG neurons was first clearly apparent seven days following application of disulfiram-loaded liposomes. Moreover, shrunken nuclei, a characteristic marker of cells undergoing apoptosis, were observed in some neurons (Figure 5.11).

S100 protein is a known marker of Schwann cells and was used for further analysis. Comparison of samples from disulfiram-treated and untreated ears confirmed the presence of a reduced number of Schwann cells in the cochleas of mice treated with disulfiram-loaded liposomes. Quantitative assessment on the basis of stereology analysis (optical dissector) indicated a loss of 50% of the Schwann cells in sections from the cochleas of the liposomes-treated mice. The loss was first observed 7 days after injection in the basal and middle cochlear turns. No apparent differences were found in the amount of cochlear damage in different animals treated with disulfiram-loaded liposomes. Fluorescent immunostaining of active caspase 3 demonstrated that cell death in the SG of mice treated with disulfiram-loaded liposomes begins shortly after the injection. Activation of the effector caspase 3 in the Schwann cells and SG neurons was observed as early as two days following the injection of liposomes. Further progression of apoptotic cell death was observed at 7 days following injection. Apoptosis indicated by active caspase 3 was not observed in the organ of Corti or in the lateral wall. Cresyl violet staining at 2 and 7 days following application of disulfiram-loaded liposomes showed damage to the fibres of SG neurons (Figure 5.11).

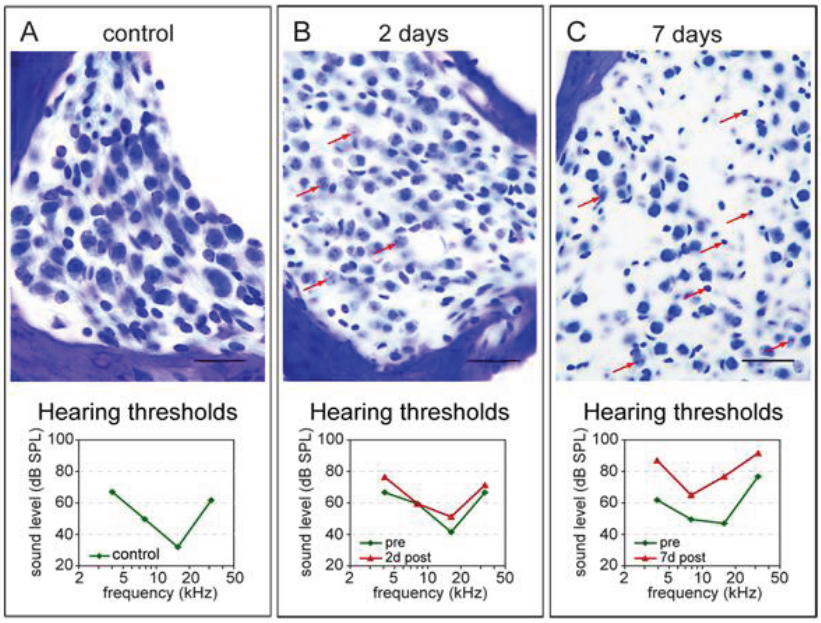

Figure 5.11: Detection of apoptosis in the SG cells with Nissl staining. Cresyl violet staining of the SG in a control mouse (**A**), in mice two days (**B**) and seven days (**C**) following the administration of disulfiram-loaded liposomes on the RWM. Lower graphs show hearing thresholds measured in the same animals before and after liposomes application. Red arrows in **B** and **C** point out examples of apoptotic cells with shrunken nuclei or the presence of 2-3 small dark dots in a cluster. Scale bar = 20 μm.

The number of intact SG neurons in individual cochlear turns was evaluated at intervals after the application of disulfiram-loaded liposomes (Figure 5.12A). Only neurons without any signs of apoptosis were considered intact. Evident loss of SG neurons was observed as early as two days after liposome application. The percentage of surviving neurons without signs of apoptosis in individual cochlear turns was 56-68% ($p<0.001$-0.05, one sample t-test against 100%). The neuronal damage continued, reaching average values of 31-47% of surviving neurons at one week post-application. However, the decrease in the number of surviving neurons observed in the second week post-application was minimal. The results indicate that RWM application was sufficient to produce a toxic effect within one week of the application of disulfiram-loaded liposomes.

5.2.2.2 *Effects of disulfiram-loaded liposomes on hearing thresholds*

The pronounced loss of SG neurons observed after disulfiram-loaded liposomes treatment was accompanied by a significant increase in the animal's hearing thresholds. The average hearing thresholds measured in animals before and two weeks after disulfiram-loaded liposome administration are shown in Figure 5.12B. In the treated animals, significant threshold shifts (20-30 dB) were present at 8 and 16 kHz. Threshold shifts were also present at 4 kHz; however, they were not significant. No hearing loss was found in contralateral untreated controls (Figure 5.12B). The results of auditory brainstem response (ABR) studies are in agreement with the histological data showing the distribution of disulfiram-loaded liposomes in all cochlear turns.

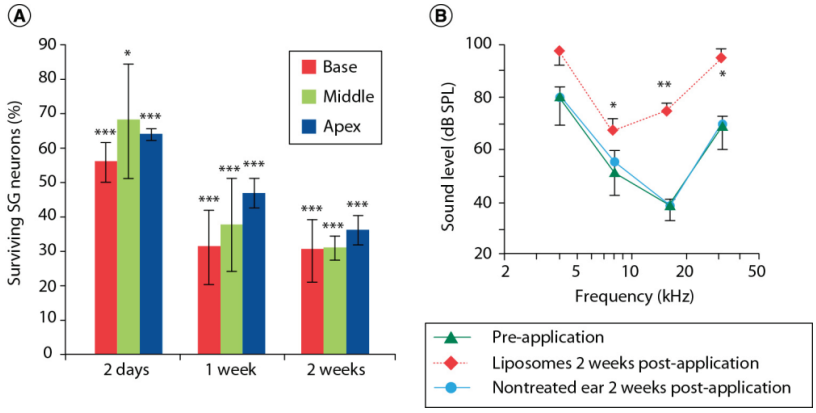

Figure 5.12: Effects of disulfiram-loaded liposomes
(**A**) The percentage of surviving SG neurons in individual cochlear parts evaluated over two weeks after disulfiram-loaded liposomes application. Each column represents amount of surviving cells averaged from 6 samples (two cochleas) (**B**) The average hearing thresholds evaluated before the disulfiram-loaded liposomes application (green full line with triangles, n=7), from contralateral untreated ears (blue full line with circles, n=7), two weeks after liposome (red dotted line with diamonds, n=3) application. Error bars represent +/- SD. * $p<0.05$, ** $p<0.01$, one-way analysis of variance with Bonferroni's multiple comparison test.

In this study, we demonstrate that liposomes applied to the round window niche of mice can penetrate through the RWM and enter cells within the cochlea. Long-term monitoring of ABRs, together with morphological evaluation of cochlear tissues, confirms that unloaded liposomes are not overtly toxic to cochlear structure or function. However, the administration of disulfiram-loaded liposomes to the RWM resulted in

significant hearing loss and pronounced structural alterations in SG cells. The damaging effect of the disulfiram-loaded liposomes indicates that the amount of liposomes that penetrated the inner ear was sufficient to affect the function of the cochlea.

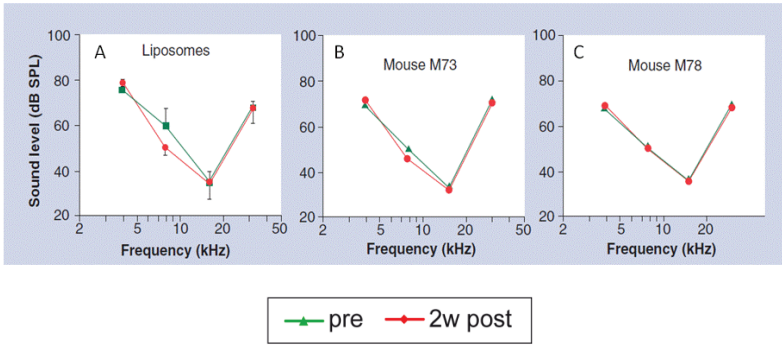

Figure 5.13: Average hearing thresholds evaluated in mice before and 2 weeks after the RWM application of drug-free liposomes (**A**, n=4). Error bars represent +/- SD. Nontoxicity of free disulfiram application on the RWM (**B** and **C**). Hearing thresholds were evaluated in two mice before and 2 weeks after the RWM application of free disulfiram.

In our study, no cochlear toxicity was observed after *in vivo* administration of drug-free liposomes (Figure 5.13 A). To exclude the possibility that the toxic effect was produced by free disulfiram that diffused out of the liposomes into the medium prior to the application, two control mice received a solution of disulfiram in saline to their RWM. No threshold shift was observed either of the control animals when tested up to two weeks post-application (Figure 5.13, B and C). These results demonstre that the morphological alterations and the pronounced hearing loss observed in the mice treated with disulfiram-loaded liposomes were produced by the disulfiram released from liposomes within the cochlea.

5.3 Liposome-mediated gene transfection and neurotrophin targeting

5.3.1 Gene expression in defined cell types

Deafness is a global medical problem affecting a large part of the human population. One of its major causes is so-called neural deafness, which involves either or both the auditory receptor cells and the auditory nerve. The ability to protect and/or regenerate these cell components would represent a major achievement in modern medicine. Because these cells are "hidden" in the bony enclave of the temporal bone, a means of directly targeting chemicals to area in which the cell lie would be an advantage. One potential way to accomplish this is the use of nanoparticles that selectively target surface molecules expressing by these specialised cells. The neurotrophin receptor tropomyosin-related kinase (Trk) receptor tyrosine kinase, especially its TrkB variant, is expressed in SG cells. TrkB plays multiple roles in signal transduction in neurons and tumour cells. Its suppressive targeting is considered in neuroblastoma and in other tumors, as well as its beneficial role is expected in neuronal survival targeting [Schimmang et al. 2003; Geiger et al. 2007]. The mouse atonal homologue Math1 was reported to be the master regulatory gene involved in the development of cochlear hair cells and neurons in both the mice and rats [Bermingham et al. 1999; Helms et al. 2000; Zheng et al. 2000; Zine et al. 2001; Chen et al. 2002; Jones et al. 2006]. Experimental overexpression of Math1 has been shown to induce the generation of new hair cells *in vitro* [Zheng et al. 2000; Woods et al. 2004] and *in vivo* [Kawamoto et al. 2003; Izumikawa et al. 2005; Gubbels et al. 2008]. Math1-based gene therapy to produce functional supernumerary hair cells in mouse [Gubbels et al. 2008] and to restore hearing in guinea pigs deafened by ototoxic drug [Izumikawa et al. 2005] has been proposed.

In our previous study, different cell types were transfected using liposomes containing Math1 plasmids [Zou et al. 2009; Zhang et al. 2011] Apart from cell culture, cochlear explants and *in vivo* transfection efficiencies were also assessed [Zou et al. 2009]. Liposomes containing the Math1 plasmid expressed the gene with variable efficiencies in the different systems tested. Efficient internalisation was observed in primary cochlear cell culture, and uptake of liposomes into SG cells and adjacent nerve fibers was observed. Due to the low tranfection efficiency of liposomes in these cell types, we designed PCL that specifically bind the TrkB receptor. This approach was chosen to enhance gene expression by targeted delivery.

Potential targetability with TrkB affinity peptide-functionalised liposomes was observed in the adult rat cochlea. Efficient gene expression was observed for the A371 (TrkB targeting) peptide-functionalised liposomes, and the function of the shRNA (to transiently silence inhibitor of differentiation and DNA binding-2, Id2) was demonstrated in cochlear explants and adult rat cochleae. shRNA [Zou et al. 2009]. Peptides that bind TrkB have been developed using either molecular modelling or phage display with the aim of mimicking the biological functions of brain-derived neurotrophic factor (BDNF) and nerve growth factor. In order to target more efficiently TrkB receptor, different ligands (peptides) were designed and conjugated to the surface of liposomes.

5.3.2 Preparation of targeted liposomes

5.3.2.1 Coupling of targeting peptides to DSPE-PEG (2000) maleimide

DSPE-PEG(2000) maleimide and the targeting peptides were mixed at a 1:1.3 molar ratio and incubated in a reaction mixture containing 100 mM Hepes, pH 7.0 and methanol (1:1.11 volume ratio) for 3 h at room temperature with constant stirring. Lipid-peptide conjugates were purified by HPLC on a reverse-phase column (Jupiter 5µm C4 300A ST 4.6/150, Amersham Biosciences, Uppsala, Sweden) eluted with a linear gradient of 0 to 100% acetonitrile in 0.1 % TFA water at a flow rate of one mL/min. Fractions containing the lipid-peptide conjugate were collected and lyophilised. The quantities of lipid-peptide conjugates were calculated by measuring the area under the peaks observed in HPLC using computer software provided by the supplier. Lipid-peptide conjugates were dissolved in methanol for use in subsequent experiments.

5.3.2.2 Incorporation of peptide-PEG-lipid conjugates into liposomes

Appropriate amounts of lipid stock solutions and the required lipid-peptide conjugate were mixed to obtain the desired compositions. Lipid films composed of Sph, eggPC, DSPE-PEG-2000, peptide-PEG-lipid conjugate, and DPPRho (0.5:0.44:0.02: 0.01: 0.03 molar ratio) were prepared. The solvent was removed under a stream of nitrogen, and the lipid residues were subsequently maintained under reduced pressure for at least 2 h. The

dry lipid film was then hydrated at 60 °C for one hour in 5 mM Hepes, 0.1 mM EDTA, pH 7.4. The lipid dispersion, at a final concentration of 0.1 mM, was subjected to AFU for 5 min using instrument settings of DC 20, intensity 10 and 500 CPB. The Z_{av} and PDI of PCL were determined by DLS at 25 °C (Table 5.2).

Table 5.1: Sequence of peptides used for neurotrophin targeting

Peptide code	Peptide sequence
A366	CSMAHPYFAR-hb-Fluorescein
A367	CRALIVFTPT-hb-Fluorescein
A368	CRANIGGTHA-hb-Fluorescein
A369	CRTMLLALLF-hb-Fluorescein
A370	CSPGSIHTLV-hb-Fluorescein
A371 (TrkB targeting)	CTFVKALTMDGKQAAWR
Scr-A371 (scrambled control for A371)	CWVLTGFTADRAKQMKA
A415 (TrkB targeting)	CENLYFQSGSMAHPYFAR [a]
Scr-A415 (scrambled control for A415)	CENLYFQSGAYHMSAPFR [a]
A417 (retro-inverse sequence of A415)	CENLYFQSGRAFYPHAMS [a]

hb: hydrazine bridge
[a]The peptides have identical amino acid compositions, as well as identical N terminal sequence CENLYFQSG, which contains the TeV protease cleavage site (between Q and S).

Table 5.2: Z-average diameters and polydispersity of control liposomes and PCL

Preparation	Size (nm)	PDI
Control liposomes (no peptide)	90 ± 5	0.220±0.010
A371-PCL	110 ± 10	0.170±0.015
Scr-A371-PCL	200 ± 100	0.270±0.020
A415-PCL	91 ± 10)	0.420±0.050
Scr-A415-PCL	98 ±20	0.264±0.020
A417-PCL	82 ±20	0.373 ± 0.20

Z_{av}, both with and without the targeting peptide were determined by DLS and reveal the liposomes to be monodisperse, with narrow particle size distributions.

5.3.3 Math1 expression in cochlear explants and cochlear cell populations

In our previous study, functionalised liposomes carrying the plasmid Math1 were tested in cochlear explants [Zou et al. 2009]. In that study dynamic uptake of liposomes in both neurofilaments and SG cells was observed, with liposomes accumulating in the SG satellite cells and gradually appearing on the neurofilaments and in the SG cells. An abundant distribution of liposomes was observed in the neurofilaments. Potentially aggregated enhanced green fluorescent protein (EGFP) expression was observed in the explants on day 2 posttreatment with A371-functionalised liposomes carrying the pGeneClipTM hMGfp plasmid DNA encoding shRNA to transiently silence id2. More EGFP expression was detected on day 4 post-treatment. Only sparse EGFP expression was detected in the explants on day 4 post-treatment with blank liposomes carrying the same plasmid DNA as the A371-functionalised liposomes. In general, EGFP expression was inefficient [Zou et al. 2009].

In the adult rat cochleae that received RWM permeation with A371-functionalised liposomes, greater nanoparticle distribution was observed in the SG region than in the cochleae treated with blank liposomes. This difference was not statistically significant, however, possibly due to the small sample size. Sparse, dot-like EGFP expression was detected in the SG cells and SG satellite cells with nanoplex internalization. In the inner hair cell region, there was significantly greater uptake of functionalised liposomes than blank liposomes. Lipoplex uptake was also observed in the lateral wall, including the spiral ligament and stria vascularis, but in these tissues uptake of the functionalised and blank liposomes was not significantly different. No uptake was detected in the outer hair cell region in cochleae treated with either A371-functionalized liposomes or blank liposomes [Zou et al. 2009].

Roy et al. [2010] recently showed that peptide A371 is identical to peptide hNgf_EE, which specifically targets TrkB and p75NTR receptors. Yet, specificity for TrkB cannot be claimed. Therefore, our next TrkB-targeting peptide, A415, was based on peptide A366, a peptide developed by Ma et al. [2003] using TrkB-expressing NIH 3T3 cells and a phage-displayed random peptide library. A366 antagonises the activity of BDNF in a dose-dependent manner and is more TrkB-specific than A371, which may also bind to p75. Peptide A371 preferably binds to TrkB and also binds to p75 receptors, while peptide A415 is able to antagonise BDNF and is thus more TrkB-specific. For this reason we selected A415 and not A371 for further

study. We deliberately avoided peptides that have physiological activity and utilised peptides with demonstrated affinity for the TrkB receptor [Ma et al. 2003]. In addition, we changed the sequences of the peptides to ensure easy and unambiguous conjugation as well as controlled release of the peptides from the surface of the PCL.

5.3.4 Binding of peptides to TrkB-positive cells

Testing of the specificities and affinities of the targeting peptides was performed using RAW264 cells, which express the TrkB receptor and K562 cells which are TrkB-negative but positive for the closely related TrkA receptor [Garcia-Suarez et al. 1998]. Fluorescein-labeled A366, A367, A368, A369, A370 and A371 peptides were added to a suspension of RAW264 or K562 cells at a concentration of 0.1 μg per 10^6 cells and incubated for 20 min at room temperature. Because peptides A367 and A369 proved to be water-insoluble after initial trials they were excluded from further analysis. All of the other designed peptides tested showed more binding to RAW264 cells than to K562 cells (Table 5.3).

Table 5.3: Binding of designed peptides to TrkB+ and TrkA+ cells, with relative specificities given as the TrkB+/TrkA+ ratio. The numbers relate to mean value for fluorescence intensity ± coefficient of variation and are given in the customary arbitrary fluorescence units (au).

	RAW264	K562	RAW264/K562 Ratio
autofluorescence	11.28 ± 64.37	18.67 ± 66.71	
A366	1296.03 ± 45.88	403.02 ± 48.44	3.22
A368	1217.71 ± 43.06	626.78 ± 46.78	1.94
A370	616.14 ± 80.27	581.78 ± 45.55	1.06
A371	486.27 ± 130.25	265.88 ± 96.1	1.83

Based on the RAW264/K562 ratio for the binding of the peptides to cells, peptide A366 exhibited the highest specificity for the TrkB receptor (Table 5.3). The peptides are expected to have lower selectivity than antibodies. Accordingly, it was important to compare binding of the peptides with binding of TrkB-specific antibodies. Both A366 and A371 showed good colocalisation with the commercially available fluorescently-labeled monoclonal antibody, 4D3F10 (Figure 5.14, A–F). These results were quantitatively confirmed by flow cytometry, revealing a good correlation between the signals from labelled antibodies and A366 (Figure 5.14G).

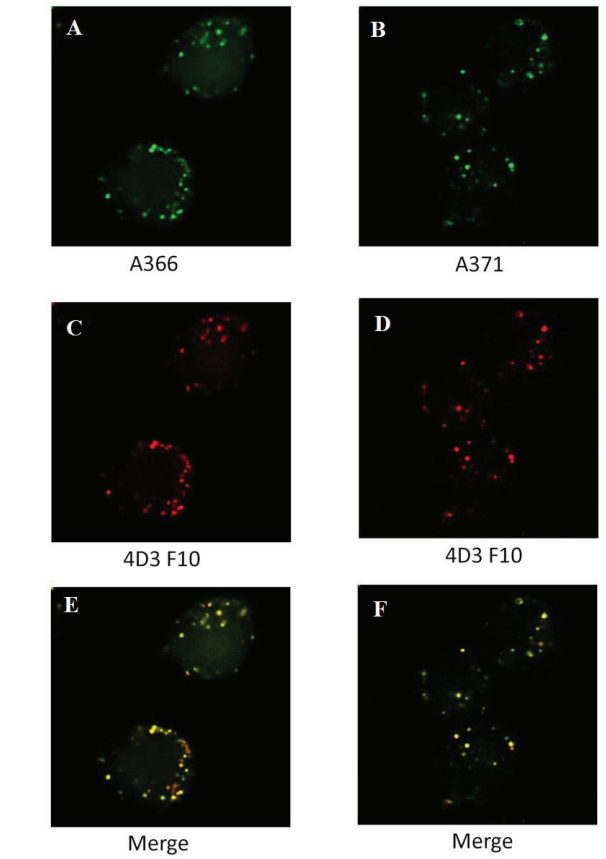

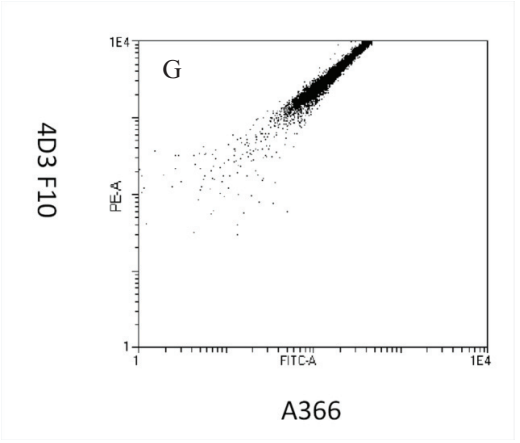

Figure 5.14: (**A–F**) Colocalization of fluorescein-labeled TrkB binding peptides (A366 and A371, green) and Alexa 633-labeled monoclonal anti-TrkB antibodies (red) to RAW264 cells. (**G**) Two-dimensional fluorescence activated cell sorting (FACS) plot made with similarly stained RAW264 cells. FITC-A, fluorescein isothiocyanate-labeled A366 peptide; PE-A, phycoerythrin-conjugated AD3F10 antibody.

5.3.5 Binding and internalisation of PCL by cultured cells

Peptides A415, Scr-A415, and A417 were developed from peptide C1 (CSMAHPYFARC), which was obtained from phage display of a custom library against NIH 3T3 cells expressing the full-length rat TrkB receptor [Ma et al. 2003]. A415 (CENLYFQSGSMAHPYFAR) contained the cysteine-truncated binding sequence of C1 with a cleavage site for TeV protease added to the N-terminus (CENLYFQSG, cleavage between Q and S). The addition of the TeV cleavage site and conjugation to liposomes could perturb the receptor-binding properties of this peptide. To check for possible interference, the binding of liposomes containing peptides A415, Scr-A415, and A417 covalently coupled to the PEG-lipid to RAW264 and K562 cells was studied. Liposomes with A415 and A417 showed binding specificity similar to that of the original peptide A366 (Figure 5.15).

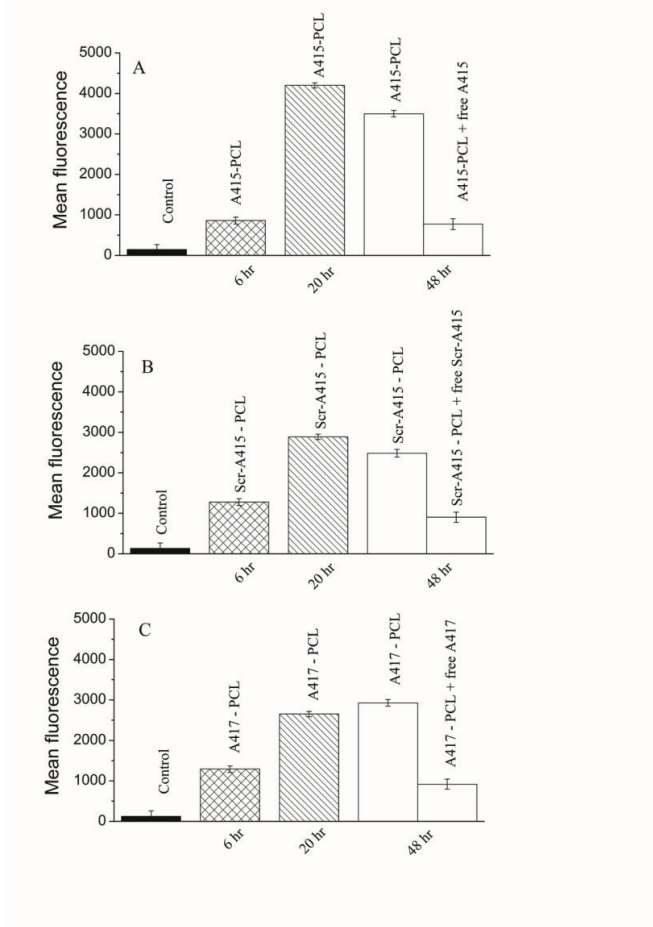

Figure 5.15: (**A**) Binding of A415-PCL to TrkB positive cells (6 or 20 h). Binding of A415-PCL to TrkB-positive cells in the presence (1 mM) or absence of competing free peptides (48 h). (**B**) Binding of Scr-A415-PCL to TrkB-positive

cells (6 or 20 h). Binding of Scr-A415 PCL to TrkB-positive cells in the presence (1 mM) or absence of competing free peptides (48 h). (**C**) Binding of A417-PCL to TrkB-positive cells (6 or 20 h). Binding of A417-PCL to TrkB-positive cells in the presence (1 mM) or absence of competing free peptides (48 h). Control depicts the level of background fluorescence of the cells.

To distinguish between binding and internalisation, 100E per mL of TeV protease (Invitrogen) was added to the cells during incubation with PCL at various time points (0 min, TeV protease added at the same time as liposomes). PCL bound to the cell surface via interaction between the peptide and TrkB receptors could be released by TeV protease, which cleaves the peptide from the liposome. However, once PCL were internalised, treatment with TeV no longer influenced the fluorescence signal from the cells. Our data suggest that the A415-conjugated liposome internalisation begins at 20 min after liposome transfection and that at 6h post transfection the majority of liposomes are internalised (Figure 5.16). PCL were tested for toxicity using standard toxicological assays and were found to be nontoxic even at concentrations higher than those used in the present study.

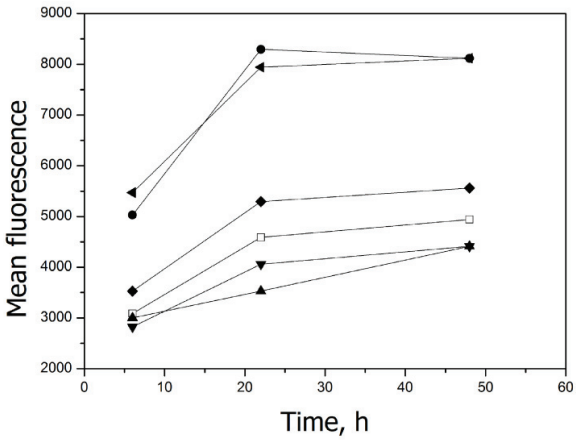

Figure 5.16: Early cleavage of the targeting peptide reduces internalization of PCL. Fluorescent A415 PCL were treated with TeV protease at 0, 20 min, and one and 6 h after their addition to the cell cultures and fluorescence intensities were measured at 6, 22, and 48 h after the addition of PCL. Control liposomes without peptide (□), A415-PCL (●), A415-PCL+TeV (0 min, ▲), A415-PCL+TeV (20 min, ▼), A415-PCL+TeV (one hour, ♦), and A415-PCL+TeV (6 h ◀).

5.3.6 Kinetics of PCL binding to cells

To understand better the relationship between binding and internalisation of PCL, we analyzed PCL binding in real time by FACS. A415 and Scr-A415 harboring PCL were added to a suspension of RAW264 cells and measurements were taken continuously over a 20-min period. The results reveal significantly faster kinetics of binding for the liposomes with the covalently coupled targeting A415 peptide compared with the scrambled Scr-A415 peptide (Figure 5.17).

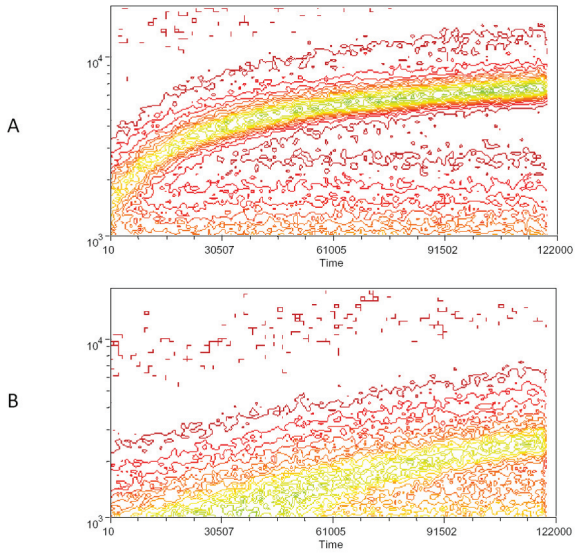

Figure 5.17: Kinetics of binding of PCL with fluorescein-labeled A415 (**A**) or the scrambled peptide Scr-A415 (**B**) added into a suspension of RAW264 cells with constant rotation. Fluorescence of individual cells was monitored for 20 min by FACS and is illustrated as a contour plot, with time in seconds (×100) on horizontal axis and number of binding events on the vertical axis, with colors representing relative density of cells in each location within the plot showing increasing frequency from red to green. The data show significantly faster binding kinetics for the liposomes with the covalently coupled targeting peptide A415 compared with the scrambled peptide.

5.3.7 Uptake of liposomes by TrkB$^+$ SH-SY5Y cells

To further assess the specificity of PCL, DPPRho-labelled PCL were added to differentiated, all-trans retinoic acid (ATRA)-treated SH-SY5Y cells and incubated for a periods of 20 min to 4 h. Selective uptake of A415-PCL by ATRA-treated SH-SY5Y cells was evident; the cells showed cytoplasmic localisation of A415-PCL after a short incubation (20 min) at 2 μM total

lipid concentration. Scr-A415-PCL were used as a control for the A415-PCL. At later time points (4 h), Scr-A415-PCL were also detected in cells (Figure 5.18).

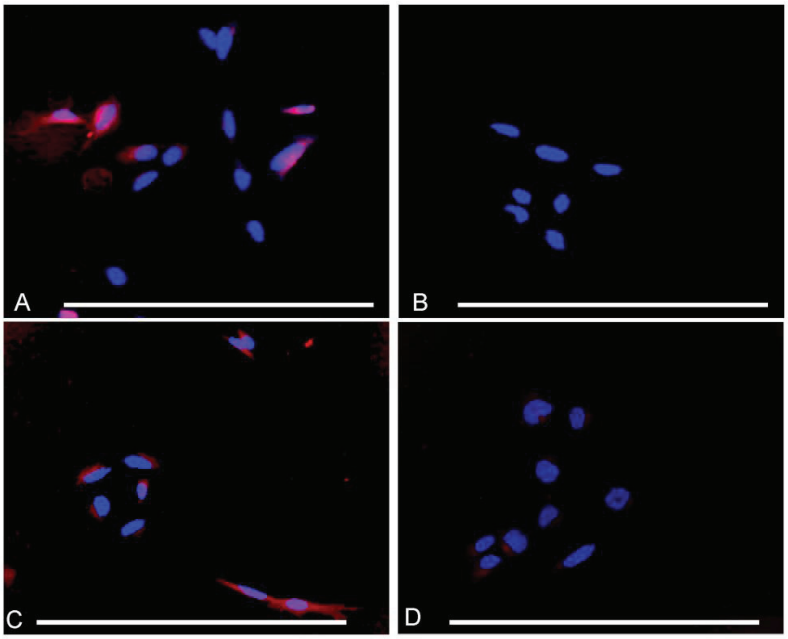

Figure 5.18: Selective uptake of A415-PCL by ATRA-treated SH-SY5Y cells, the selectivity being dependent on incubation time. (**A**) ATRA-treated SH-SY5Y cells incubated with A415-PCL for 20 min. (**B**) ATRA-treated SH-SY5Y cells incubated with Scr-A415-PCL for 20 min. (**C**) ATRA-treated SH-SY5Y cells incubated with A415-PCL for 4 h. (**D**) ATRA-treated SH-SY5Y cells incubated with Scr-A415-PCL for 4 h. Red: DPPRho-labeled PCL, Blue: nuclear counterstaining (DAPI). Bar corresponds to100 μm.

SH-SY5Y cells are the third successive subclone of the SKN-SH human neuroblastoma cell line and were purchased from the Health Protection Agency Culture Collection (Salisbury, UK). When treated with ATRA, SH-SY5Y cells develop a distinct phenotype, with morphological changes and expression of biochemical and functional markers resembling those of neurons [Encinas et al. 2000]. SH-SY5Y cells are frequently used as a model for studying the molecular mechanisms involved in neuronal differentiation. Treatment of SH-SY5Y cells with ATRA induces the expression of TrkB (NTRK2) but not of TrkA (NTRK1), and thus becomes responsive to BDNF and NT-4/5 neurotrophins [Encinas et al. 2000].

We further investigated the intracellular localisation of A415-conjugated liposomes in TrkB+ SH-SY5Y cells using antibodies for early endosomal antigen 1 protein which binds phospholipid vesicles containing phosphatidylinositol 3-phosphate (anti-early endosomal autoantigene-1

IgG), We detected partial colocalisation of early endosomes and A415-conjugated PCL (Figure 5.19).

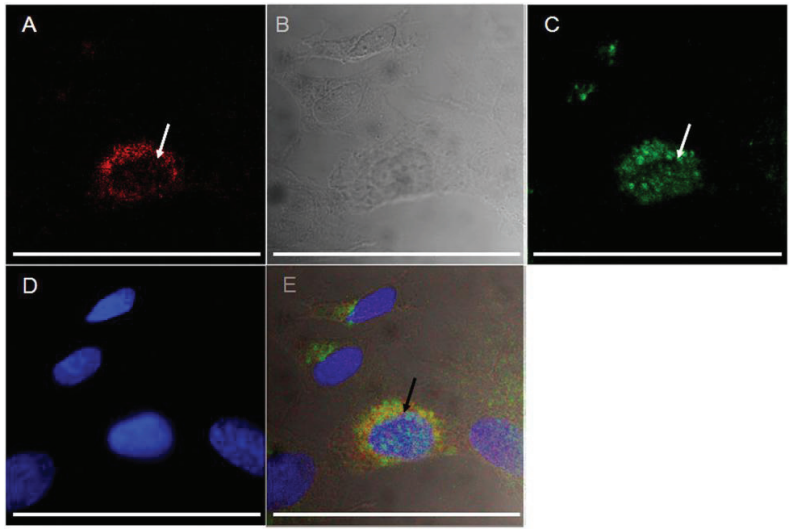

Figure 5.19: Uptake of A415-PCL by ATRA-treated SH-SY5Y TrkB+ cells after 8 h of incubation, showing partial colocalization with the anti-early endosomal 1 antibody (*arrows*). Fluorescence of A415-PCL-labeled with TRITC (**A**), differential contrast image (**B**), immunocytochemistry of early endosomal autoantigene-1 (fluorescein isothiocyanate-labeled, (**C**), nuclear counterstaining (DAPI) (**D**), and merge of panels **A–D** (**E**). Bar illustrates 100 μm.

Our data demonstrate that certain structural modifications do not hamper the TrkB-binding activity of the peptides used in this study and that these modifications could allow PCL to deliver cargo to different TrkB+ cell types. Depending on their cargo, these PCL could provide an efficient means for administering drugs that increase the survival of neuronal tissues or for proapoptotic treatment of neoplasms, conveying either antiapoptotic or proapoptotic agents, respectively.

5.4 MRI-traceable liposomes and inner ear visualisation

5.4.1 Liposomes containing MRI contrast agent

5.4.1.1 Liposomes containing DMPE-DTPA(Gd)

In developing our integrated imaging approach, we decided to use a lipid tagged with gadolinium to visualise liposomes within the inner ear. Accordingly, appropriate lipids, along with DMPE-DTPA (Gd) (Gd chelate lipid), were mixed; the solvent was evaporated under nitrogen to obtain a thin lipid film that was subsequently dried overnight under vacuum. The lipid film was hydrated with buffer, and the resulting MLV were then sequentially extruded from 400 nm (five times), 200 nm (five times), and 100 nm (seven times) pore size polycarbonate Millipore filters to yield unilamellar liposomes containing gadolinium in both leaflets.

Gadolinium (Gd), with its 7 unpaired electrons in 4f orbitals that provide a very large magnetic moment, has been shown to be among the best agents for contrast-enhanced MRI [Bui et al. 2010]. We prepared two different types of MRI-traceable liposomes. First, to determine whether a biocompatible lipid nanoparticle with surface bound Gd can improve MRI contrast sensitivity, we constructed liposomes containing DMPE with bound DTPA chelating Gd (Figure 5.20).

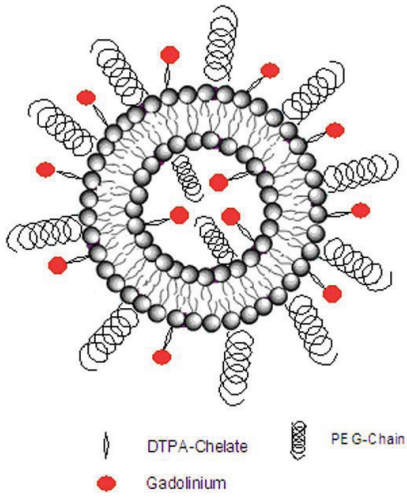

Figure 5.20: Schematic representation of liposome containing gadolinium chelate lipid.

5.4.1.2 Liposomes encapsulating Gd-DOTA

The second type of MRI-traceable liposomes we developed are liposomes encapsulating Gd-DOTA (Figure 5.21). To obtain these liposomes lipids were dissolved in chloroform and the solvent was subsequently removed under a gentle stream of nitrogen. The dry lipid residues were then maintained under reduced pressure for at least 24 h to remove trace amounts of chloroform. The lipid film was hydrated with Gd-DOTA solution (500 mM) at 60°C for 60 min. The resulting lipid suspensions were extruded through 400 nm (five times), 200 nm (five times), and 100 nm (seven times) polycarbonate Millipore filters to yield LUV containing Gd-DOTA both inside and outside the liposomes. After extrusion, external gadolinium was removed by passage of the liposomes suspension through Sephadex G-50 (fine) quick spin columns (Roche Diagnostics GmbH, Mannheim, Germany).

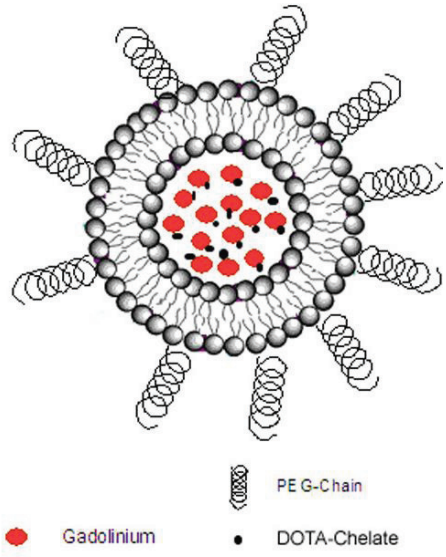

Figure 5.21: Schematic representation of liposome encapsulating Gd-DOTA

5.4.2 Characteristics of MRI-traceable liposomes

5.4.2.1 DLS

The average particle sizes of liposomes tagged with Gd-DTPA or encapsulating Gd-DOTA were measured (Figure 5.22). Liposomes

containing Gd-DTPA showed a more dispersed size distribution. For liposomes encapsulating Gd-DOTA, Z_{av} values of 300 ± 20 and 130 ± 20 nm were obtained before and after removal of the external Gd-DOTA. All liposomes encapsulating Gd-DOTA (500 mM) were stable for at least one week after preparation as confirmed by DLS, revealing no changes in Z_{av}.

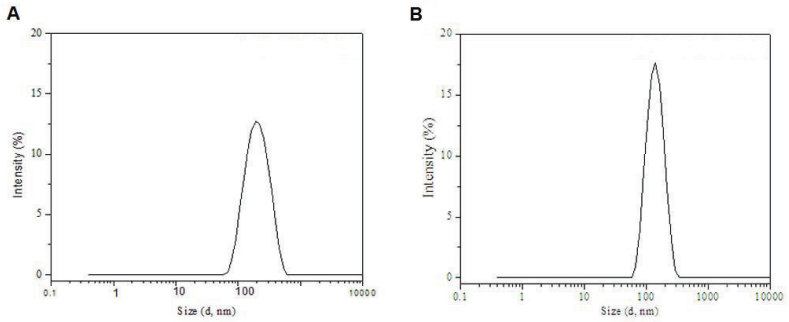

Figure 5.22: Size distribution by intensity of purified liposomes (total lipid concentration 1 mM) containing Gd-DTPA or encapsulating Gd-DOTA obtained by DLS. Temperature was maintained at 25°C. liposomes containing Gd-DTPA (**A**) showed more dispersed size distribution than liposomes encapsulating Gd-DOTA (**B**).

5.4.2.2 Phantom study

To evaluate the T1 and T2 relaxation times of liposomes containing Gd-DTPA and to analyse the contribution of water-accessible Gd-DTPA to the MR signal, liposome solutions (1 mM) were prepared in physiological saline containing 0.5 mM Gd. To disassemble the liposomes and expose all the lipid-bound Gd-DTPA to the water, 3 - 5% SDS was added to the solution. This was performed so that the MRI signal from all of the Gd-DTPA associated with the liposomes, including the amount within the liposomes that was shielded by the lipid from proton interaction, could be detected. Gd-DOTA diluted with physiological saline at a concentration of 0.5 mM was used as a positive control. Plastic phantom tubes (400 µl, AgnTho's AB, Sweden) were filled with the solutions of Gd-DOTA, liposomes containing Gd-DTPA, or liposomes containing Gd-DTPA plus 5% SDS. To measure the relaxivities, r1 and r2, of liposomes encapsulating Gd-DOTA, solutions of various concentrations were filled into plastic phantom tubes and then placed in the centre of a 50-ml syringe. Dilutions were made with artificial perilymph containing 145.5 mM NaCl, 2.7 mM KCl, 2.0 mM MgSO4, 1.2 mM CaCl2, 5.0 mM HEPES, pH adjusted to 7.4 [Takemura et al. 2004].

Negative controls were prepared using either plain artificial perilymph or HEPES buffer. Each sample was prepared in duplicate.

The T2 relaxation time was determined using a multi-slice multi-echo sequence (MSME) based on CPMG (Carr-Purcell Meiboom-Gill) spin echo (SE) [repetition time (TR) 1500 ms, echo time (TE) 7-229 ms, 32 echo times, matrix size 128 × 128, single slice, slice thickness 2.0 mm, field of view (FOV) 5.0 cm, resolution 0.098 × 0.130 mm2, number of excitation (NEX) 3]. T1 relaxation times were determined by rapid acquisition with relaxation enhancement (RARE) sequence with variable TR (TR 100, 432, 859, 1458, 2472, 7500 ms, TEeff 8.7 ms, RARE factor 2, NEX 1, matrix size 128 × 128, FOV 5 cm, single slice with slice thickness 2.0 mm).

In phantom testing, liposomes tagged with Gd-DTPA showed characteristics of a T1-contrast agent, but the maximum available concentration of the liposomes did not produce sufficient signal intensity for *in vivo* application. Liposomes tagged with Gd-DTPA and dissociated by 3 - 5% SDS demonstrated T1 and T2 relaxation times similar to Gd-DOTA at the same molar concentration of Gd (Table 5.4). T1 signal enhancement correlated with the amount of water accessible to the gadolinium, shown by the fact that SDS treatment induced a T1 relaxation time of liposomes tagged with Gd-DTPA equivalent to that of Gd-DOTA at the same concentration. It has been reported that Gd-DTPA and Gd-DOTA showed similar relaxivities [Bousquet et al., 1988]. Gd-DTPA requires relatively high doses of Gd; thus, Gd contrast agents that produce higher resolution images using a much lower Gd dose could address both imaging sensitivity and Gd safety. Because the ratio of Gd chelate to lipid within the material was already maximised in the first type of magnetic liposomes, an alternative strategy was pursued to enhance the r1 of the liposomes containing MRI contrast agent. For this strategy, liposomes encapsulating Gd-DOTA represented a better choice.

Table 5.4: Relaxation times of different liposomes containing MRI contrast agent at certain concentrations.

Samples	Liposome concentrations	Gd concentrations	Relaxation times (mS) (mean±SD)	
			T1	T2
Liposomes containing Gd-DTPA	1 mM	0.5 mM	1897±370	273±4
Liposomes containing Gd-DTPA + 5% SDS	1 mM	0.5 mM	1697±380	455±5
Gd-DOTA		0.5 mM	1566±324	447±5
Liposomes encapsulating Gd-DOTA (purified)*	0.00625 mM	3.125 mM	1980±11	620±7
Liposomes encapsulating Gd-DOTA (unpurified)†	0.003125 mM	1.5625 mM	184±13	102±1

*samples were diluted 160 folds; † samples were diluted 320 folds.

5.4.2.3 Cryo-TEM

Cryo-TEM of liposomes encapsulating Gd-DOTA.

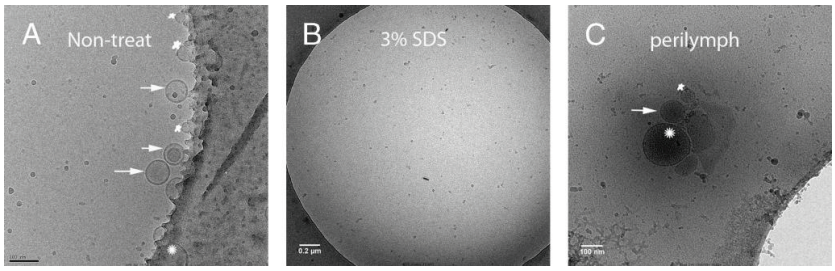

Figure. 5.23: The typical morphology of a liposome shows an electron-dense membrane with a mean size of 95 nm (*arrow*) and polydiversity (*star*, below 95 nm; *asterisk*, above 95 nm) (**A**). After dissolution of liposomes with 3% SDS, small micelle-like structures were observed; however, no 100-nm liposomes were observed (**B**). After passing through the middle-inner ear barriers, 95 nm liposomes (*arrow*) with similar polydiversity to that before delivery (*star*, below 95 nm; *asterisk*, above 95 nm) were observed in the collected perilymph specimens from the rat inner ear (**C**). Scale bar = 100 nm in **A** and **C**, 200 nm in **B**. (Adapted from ‘‘Size-dependent passage of liposome nanocarriers with preserved posttransport integrity across the middle-inner ear barriers in rats’’ by Jing Zou, Rohit Sood, Sanjeev Ranjan, et al., 2012, *Otology & Neurotology*, 33:4). Copyright 2012 by the Wolters Kluwer Health.

5.4.3 Transportation of liposomes through the middle inner ear barrier

When a 1 mM suspension of liposomes encapsulating 500 mM Gd-DOTA was applied to the middle ear cavity by transtympanic injection, liposomes containing Gd-DOTA were detected in the middle ear cavity; these liposomes caused a strong T1-weighted signal that decayed between 3 to 6 h post-administration (figure 5.24). Liposomes encapsulating Gd-DOTA were efficiently detected in the perilymph of the inner ear at 3 h post-administration; the signal from the inner ear (average of the vestibule, scala vestibuli, and scala tympani) reached 21.1% of that in the middle ear cavity (figure 5.24). After 6 h, the signal intensity from the inner ear increased slightly; although statistical significance was not achieved, this result indicates that, with the passage of time, more liposomes encapsulating Gd-DOTA entered the inner ear. Three-dimensional rendering images showed that abundant liposomes were retained in the vestibule and perilymphatic compartments of the basal lower turn. Within the cochlea, additional liposomes diffused into the higher turns of the cochlea, rendering the perilymph in the second turn and apex more visible. The signal intensity in the brainstem was also slightly enhanced at 6 h in comparison to 3 h, though without statistical significance (figure 5.24). An important phenomenon was noticed in that the uptake of purified liposomes encapsulating Gd-DOTA in the inner ear was influenced by the posture of the animal after transtympanic injection. To be able to perform scanning immediately following injection, two rats were placed into the MRI machine in the prone position. Liposomes encapsulating Gd-DOTA were not detected in the inner ears of these animals at 3 h post-administration. However, when rats were placed in a lateral position with the exposed ear upwards for approximately 2.5 h before scanning, detectable liposomes encapsulating Gd-DOTA were present in the inner ear at 3 h post-administration (figure 5.24). Liposomes encapsulating Gd-DOTA were not detectable in the inner ear at 24 h after injection in either group of animals. Unpurified liposomes encapsulating Gd-DOTA were efficiently detected in the perilymph of the inner ear at 40 min after post-transtympanic injection.

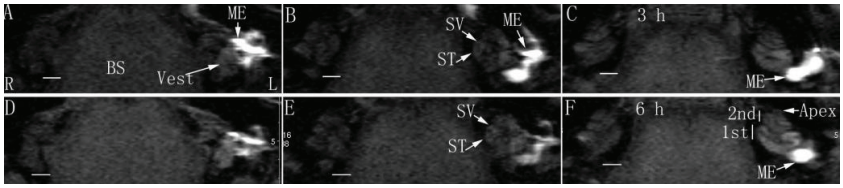

Figure 5.24: Visualisation of liposomes encapsulating Gd-DOTA in the middle ear cavity and inner ear of rat after transtympanic injection using T1-weighted 2D MRI. Liposomes encapsulating Gd-DOTA (1.0 mM liposomes encapsulating Gd-DOTA containing 500 mM Gd-DOTA) were delivered to the left middle ear. At 3 h time point (**A-C**), they were detected in the middle ear cavity, vestibule, and cochlea. Aftert 6 h (**D-F**), these regions with uptake of liposomes showed brighter signal and the second turn and apex of the cochlea became more visible. 1st: the basal turn; 2nd: the second turn; BS: brainstem; L: left ear; ME: middle ear; R: right ear; ST: scala tympani; SV: scala vestibuli; Vest: vestibule. Particle sizes = 150 ± 20 nm. Scale bar = 1 mm.

5.4.4 Distribution of MRI-traceable liposomes in the inner ear after intracochlear injection

Intracochlear administration of liposomes encapsulating Gd-DOTA with a volume 5 µl (1 mM liposomes encapsulating Gd-DOTA containing 500 mM Gd-DOTA) in a closed perilymph circulation system through a catheter failed to produce visible signal in the inner ear. 10 µl volume of the same liposomes encapsulating Gd-DOTA induced bright signal on T1-weighted images mainly in the region adjacent to the injection, that is, in the basal turn of the scala tympani, scala vestibuli, and modiolus immediately after intracochlear injection (Figure 5.25). However, no further diffusion to the distal locations of the inner ear was visualized with prolonged observation time. When 50 µl was injected, using higher pressure to drive the liposomes, a broader distribution of liposomes encapsulating Gd-DOTA in the inner ear was visualized, including the cochlea and the adjacent scala vestibuli. An abundance of liposomes encapsulating Gd-DOTA were demonstrated in the modiolus at the level of the basal turn. In the scala vestibuli, the signal intensity was lower than in the scala tympani (Figure 5.25). At 56 min, liposomes encapsulating Gd-DOTA diffused to distal sites, such as the apex of the cochlea and the semicircular canals in the vestibular organ (Figure 5.25).

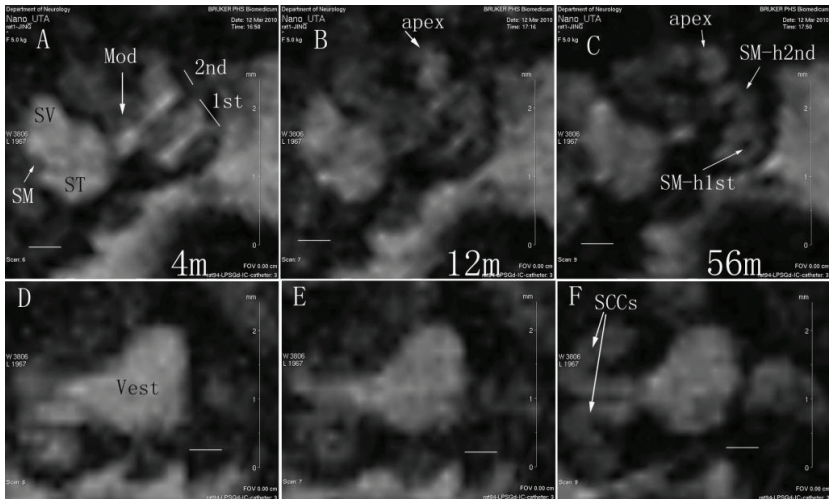

Figure 5.25: Dynamic distribution of liposomes encapsulating Gd-DOTA in the inner ear after intracochlear delivery in closed perilymphatic compartments demonstrated by MPR single view of T1-weighted 3D MRI. 1 mM liposomes containing 500 mM Gd-DOTA were administered. In the cochlea, liposomes filled SM at the beginning, but were cleaned from SM after 56 m (**A**, **B**, and **C**). In the vestibule, liposomes retained in the proximal locations of SCCs, but distributed to the distal parts of SCCs at 56 m post-injection (**D, E, F**). 1st: the basal turn; 2nd:the second turn; 4 m, 12 m, and 56 m: 4 min, 12 min, and 56 min; Mod: modiolus; MPR: multiplanar reconstruction; SSCs: semicircular canals; SM: the scala media; SM-h1st: SM of the higher basal turn; SM-h2nd: SM of the higher second turn; ST: the scala tympani; SV: the scala vestibuli; Vest: vestibule. Scale bar = 500 μm.

Intracochlear administration of liposomes encapsulating Gd-DOTA through gelatin sponge [Zou et al. 2010] applied to an open perilymph system, with windows created in both the scala vestibuli and scala tympani, induced highly intense bright signal in the inner ear on T1-weighted images acquired at 30 min (Figure 5.26). At this time point, the signal intensity in the perilymph of the vestibule was higher than in the perilymph of the cochlea, which was in turn higher than the modiolus. Homogeneous distribution of liposomes encapsulating Gd-DOTA was observed throughout the perilymphatic compartments of the cochlea. A dynamic reduction of signal in the hook region of the scala tympani and the modiolus of the cochlea was demonstrated, which became faint at 120 min post-administration (Figure 5.26). In the vestibular organ, gradual enhancement occurred in the semicircular canals over 120 min while no visible change was found in the vestibule, which remained bright throughout this period (Figure 5.26).

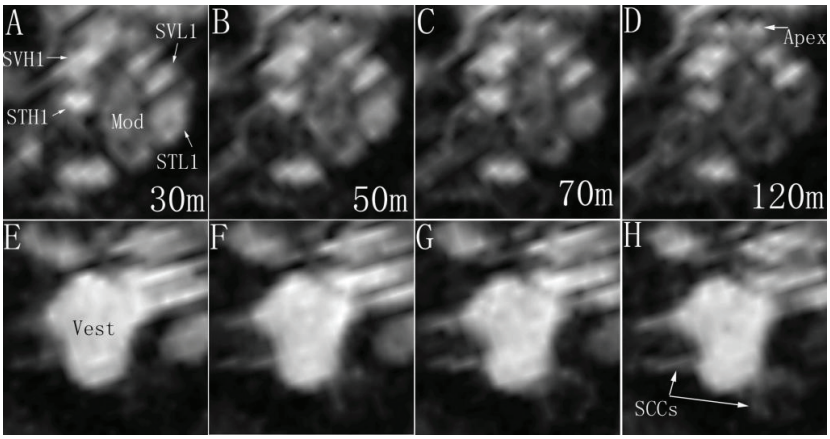

Figure 5.26: Dynamic distribution of liposomes encapsulating Gd-DOTA in the inner ear after intracochlear delivery in an open perilymphatic compartments demonstrated by MPR single view of T1-weighted 3D MRI. 1 mM liposomes containing 500 mM Gd-DOTA were administered. Intracochlear dynamics was shown in **A** through **D**; intravestabular dynamics was shown in **E** through **H**. From 30 min to 120 min postadministration of liposomes encapsulating Gd-DOTA, signal intensities decayed gradually in the STL1, STH1, and Mod; but retained stable in the SVL1, SVH1, and Vest. 30 m, 50 m, etc.: 30 min etc; Mod: modilous; MPR: multiplanar reconstruction; SSCs: semicircular canals; STH1: scala tympani of the higher basal turn; STL1: scala tympani of the lower basal turn; SVH1: scala vestibuli of the higher basal turn; SVL1: scala vestibuli of the lower basal turn; Vest: vestibule.

In the present study, novel MRI-visible liposomes were designed by encapsulating Gd-DOTA into the hydrophilic cores of the liposomes. With this method, it was possible to encapsulate 500 mM Gd into the liposomes, whereas with liposomes containing gadolinium chelate lipid, the maximum concentration of incorporated Gd was 0.5 mM. Moreover, highly monodisperse liposomes were obtained when Gd-DOTA was encapsulated into the aqueous core. The production of monodisperse liposomes is critical for quality control in pharmaceutics and correlates with treatment efficacy. It is important to note that the gadolinium within liposomes is carried in the aqueous core and that the shell can be manufactured to be identical to that of the therapeutic nanoparticles. Therefore, this MRI study is directly translatable for predicting the destination of liposomes of the type described here in clinical use to carry genes or drugs. These novel liposomes have potentially broad application in future biomedical investigations.

6. Conclusions

Liposomes have broad potential in a variety of medical applications. The nano size gives some of its exciting properties to a multifunctional liposome. Although there are several methods for preparing liposomes, we developed a method that is efficient and overcomes some of the limitations associated with other previously described methods (Publication I).

Liposomes have great potential for use in transporting a large variety of therapeutic agents, including hydrophilic and hydrophobic drugs, siRNA and DNA across the RWM into the cochlea. Liposomes are capable of carrying payloads which would not ordinarily cross the RWM or would cause morphological changes in the inner ear by doing so. The results reported in publication II demonstrate that the liposomes are capable of carrying into the inner ear a payload that elicits a biological effect with consequences measurable by a functional readout. A similar strategy could be employed to treat and prevent neural hearing loss.

The neurotrophic receptor TrkB is expressed in SG cells and the activation of these cells is important in improving inner ear neuronal cell survival and regeneration. In the original publication III, we demonstrate the feasibility of targeting liposomes to TrkB receptor-expressing cells using specific peptide-based ligands.

In the process of optimising liposome-based drug delivery to the inner ear, it is essential to be able to trace the passage of liposomes through the cochlea. In the final publication (IV), effective MRI-traceable liposomes were developed, and their distribution dynamics were studied in the inner ear of the rat.

7. Future Perspectives

Endosomal/lysosomal degradation is a major obstacle to gene transfection efficacy and drug delivery into mammalian cells. The best way to design endosomolytic peptides is presently unclear, and this currently represents a challenging issue in drug/gene delivery systems. This prompted us to design and characterise several analogues of some well-studied antimicrobial peptides. Interestingly, our preliminary results showed that the analogues we designed exhibited almost negligible toxic activity to mammalian cells at physiological pH (7.4), while they showed appreciably high toxic activity at endosomal/lysosomal pH (5.0). These findings indicate that this novel approach provides a powerful strategy and platform upon which to develop pH-sensitive potent shorter endosomolytic peptides (*manuscript in preparation*). It will be interesting to use these designed endosomolytic peptides in our liposomes for better drug/gene delivery *in vivo*. A patent filing is in process at Aalto University claiming the novel design of several endosomolytic peptides that result in enhanced gene expression in mammalian cells.

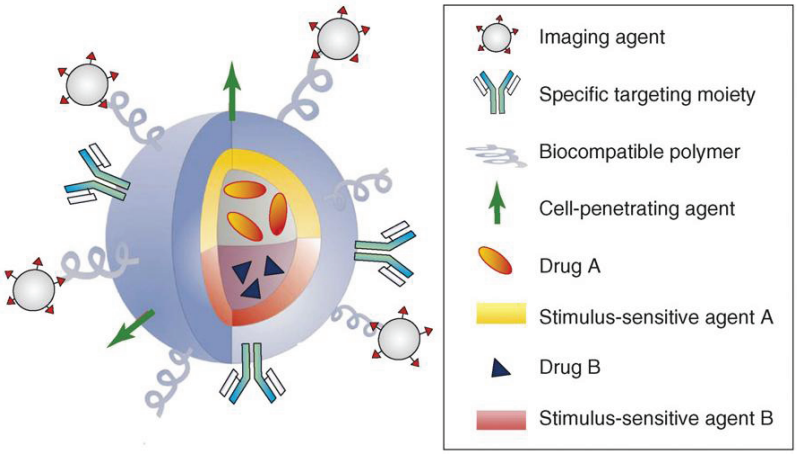

Figure 7.1: A schematic illustration of an ideal multifinctional liposome. Multifunctional liposomes could combine a specific targeting moiety (usually an antibody or peptide) with imaging agent (such as magnetic contrast agent or

quantum dots), a cell-penetrating agent (including endosomolytic peptides for endosomal escape), a stimulus-sensitive element for drug release, a stabilising polymer to ensure biocompatibility (polyethylene glycol most frequently) and the therapeutic compound. Development of novel strategies for controlled released of drugs will provide nanoparticles with the capability to deliver two or more therapeutic agents. ‘‘Reprinted from the Trends in Biotechnology, *26,* Nuria Sanvicens and M. Pilar Marco, Multifunctional nanoparticles – properties and prospects for their use in human medicine, 425-433, Copyright 2012 with permission from Elsevier.”

The use of liposomes provides opportunities for specific design and tuning properties that are not possible with other types of therapeutic nanoparticles, and as more clinical data become available. The different properties of liposomes outlined in this thesis could be combined to design liposomes that are truly multifunctional. As illustrated by the figure 7.1, we must attempt to design more sophisticated advanced multifunctional liposomes and bring these to the clinic. Interestingly, results from clinical trials are already fuelling enthusiasm for this type of therapeutic modality. Although it may be important to regulate the size advanced multifunctional liposomes used for inner ear therapy, size limitation is not extremely critical to a drug company from a formulation, delivery or efficacy perspective because the desired properties of many nanomedicinec can be achieved using a size range greater than 100 nm.

8. References

Alton EW, Stern M, Farley R, Jaffe A, Chadwick SL, Phillips J *et al.* (1999). Cationic lipid-mediated CFTR gene transfer to the lungs and nose of patients with cystic fibrosis: A double-blind placebo-controlled trial. *Lancet* **353:** 947-954.

Bagatolli LA, Parasassi T, Gratton E. (2000). Giant phospholipid vesicles: Comparison among the whole lipid sample characteristics using different preparation methods: A two photon fluorescence microscopy study. *Chem Phys Lipids* **105:** 135-147.

Baker TS, Olson NH, Fuller SD. (1999). Adding the third dimension to virus life cycles: Three-dimensional reconstruction of icosahedral viruses from cryo-electron micrographs. *Microbiol Mol Biol Rev* **63:** 862-922, table of contents.

Balda MS, Matter K. (1998). Tight junctions. *J Cell Sci* **111 (Pt 5):** 541-547.

Bangham AD, Horne RW. (1964). Negative staining of phospholipids and their structural modification by surface-active agents as observed in the electron microscope. *J Mol Biol* **8:** 660-668.

Batzri S, Korn ED. (1973). Single bilayer liposomes prepared without sonication. *Biochim Biophys Acta* **298:** 1015-1019.

Bermingham NA, Hassan BA, Price SD, Vollrath MA, Ben-Arie N, Eatock RA *et al.* (1999). Math1: An essential gene for the generation of inner ear hair cells. *Science* **284:** 1837-1841.

Bitsche M, Dudas J, Roy S, Potrusil T, Schmutzhard J, Schrott-Fischer A. (2011). Neurotrophic receptors as potential therapy targets in postnatal development, in adult, and in hearing loss-affected inner ear. *Otol Neurotol* **32:** 761-773.

Boeckle S, Fahrmeir J, Roedl W, Ogris M, Wagner E. (2006). Melittin analogs with high lytic activity at endosomal pH enhance transfection with purified targeted PEI polyplexes. *J Control Release* **112:** 240-248.

Bohne BA, Gruner MM, Harding GW. (1990). Morphological correlates of aging in the chinchilla cochlea. *Hear Res* **48:** 79-91.

Bousquet JC, Saini S, Stark DD, Hahn PF, Nigam M, Wittenberg J *et al.* (1988). Gd-DOTA: Characterization of a new paramagnetic complex. *Radiology* **166:** 693-698.

Brennen CE, *Cavitation and bubble dynamics*, Oxford University Press: New York, 1995; Chapter 1.

Bui T, Stevenson J, Hoekman J, Zhang S, Maravilla K, Ho RJY. (2010). Novel Gd nanoparticles enhance vascular contrast for high-resolution magnetic resonance maging. *PLoS ONE* **5:** 1-7.

Caplen NJ, Alton EW, Middleton PG, Dorin JR, Stevenson BJ, Gao X *et al.* (1995). Liposome-mediated CFTR gene transfer to the nasal epithelium of patients with cystic fibrosis. *Nat Med* **1:** 39-46.

Chen P, Johnson JE, Zoghbi HY, Segil N. (2002). The role of Math1 in inner ear development: Uncoupling the establishment of the sensory primordium from hair cell fate determination. *Development* **129:** 2495-2505.

Defrise QF, et al. (1984): Model studies for drug entrapment and liposome stability. In: Gregoriadis G, editor. *Liposome technology*. Vol. 2. 1st ed. Boca Raton (FL), CRC Press.

De Lima MC, Simoes S, Pires P, Gaspar R, Slepushkin V, Duzgunes N. (1999). Gene delivery mediated by cationic liposomes: From biophysical aspects to enhancement of transfection. *Mol Membr Biol* **16:** 103-109.

Donkuru M, Badea I, Wettig S, Verrall R, Elsabahy M, Foldvari M. (2010). Advancing nonviral gene delivery: Lipid- and surfactant-based nanoparticle design strategies. *Nanomedicine (Lond)* **5:** 1103-1127.

Encinas M, Iglesias M, Liu Y, Wang H, Muhaisen A, Cena V *et al.* (2000). Sequential treatment of SH-SY5Y cells with retinoic acid and brain-derived neurotrophic factor gives rise to fully differentiated, neurotrophic factor-dependent, human neuron-like cells. *J Neurochem* **75:** 991-1003.

Farhood H, Serbina N, Huang L. (1995). The role of dioleoyl phosphatidylethanolamine in cationic liposome mediated gene transfer. *Biochim Biophys Acta* **1235:** 289-295.

Felgner PL, Gadek TR, Holm M, Roman R, Chan HW, Wenz M *et al.* (1987). Lipofection: A highly efficient, lipid-mediated DNA-transfection procedure. *Proc Natl Acad Sci U S A* **84:** 7413-7417.

Fielden ML, Perrin C, Kremer A, Bergsma M, Stuart MC, Camilleri P *et al.* (2001). Sugar-based tertiary amino gemini surfactants with a vesicle-to-micelle transition in the endosomal pH range mediate efficient transfection *in vitro*. *Eur J Biochem* **268:** 1269-1279.

Garcia-Suarez O, Hannestad J, Esteban I, Sainz R, Naves FJ, Vega JA. (1998). Expression of the TrkB neurotrophin receptor by thymic macrophages. *Immunology* **94:** 235-241.

Geiger TR, Peeper DS. (2007). Critical role for TrkB kinase function in anoikis suppression, tumorigenesis, and metastasis. *Cancer Res* **67:** 6221-6229.

Goycoolea MV, Lundman L. (1997). Round window membrane. structure function and permeability: A review. *Microsc Res Tech* **36:** 201-211.

Helms AW, Abney AL, Ben-Arie N, Zoghbi HY, Johnson JE. (2000). Autoregulation and multiple enhancers control Math1 expression in the developing nervous system. *Development* **127:** 1185-1196.

Herborn CU, Honold E, Wolf M, Kemper J, Kinner S, Adam G *et al.* (2007). Clinical safety and diagnostic value of the gadolinium chelate gadoterate meglumine (gd-DOTA). *Invest Radiol* **42:** 58-62.

Horner KC, Guilhaume A. (1995). Ultrastructural changes in the hydropic cochlea of the guinea-pig. *Eur J Neurosci* **7:** 1305-1312.

Huang SK, Stauffer PR, Hong K, Guo JW, Phillips TL, Huang A *et al.* (1994). Liposomes and hyperthermia in mice: Increased tumor uptake and therapeutic efficacy of doxorubicin in sterically stabilized liposomes. *Cancer Res* **54:** 2186-2191.

Huebner S, Battersby BJ, Grimm R, Cevc G. (1999). Lipid-DNA complex formation: Reorganization and rupture of lipid vesicles in the presence of DNA as observed by cryoelectron microscopy. *Biophys J* **76:** 3158-3166.

Hui SW, Langner M, Zhao YL, Ross P, Hurley E, Chan K. (1996). The role of helper lipids in cationic liposome-mediated gene transfer. *Biophys J* **71:** 590-599.

Igarashi Y, Ishii T. (1990). Lipofuscin pigments in the spiral ganglion of the rat. *Eur Arch Otorhinolaryngol* **247:** 189-193.

Ishii T. (1977). The fine structure of lipofuscin in the human inner ear. *Arch Otorhinolaryngol* **215:** 213-221.

Janmey PA, Kinnunen PK. (2006). Biophysical properties of lipids and dynamic membranes. *Trends Cell Biol* **16:** 538-546.

Johnson SM, Bangham AD, Hill MW, Korn ED. (1971). Single bilayer liposomes. *Biochim Biophys Acta* **233:** 820-826.

Jones JM, Montcouquiol M, Dabdoub A, Woods C, Kelley MW. (2006). Inhibitors of differentiation and DNA binding (ids) regulate Math1 and hair cell formation during the development of the organ of corti. *J Neurosci* **26:** 550-558.

Kawaura C, Noguchi A, Furuno T, Nakanishi M. (1998). Atomic force microscopy for studying gene transfection mediated by cationic liposomes with a cationic cholesterol derivative. *FEBS Lett* **421:** 69-72.

Kinnunen PK, Rytomaa M, Koiv A, Lehtonen J, Mustonen P, Aro A. (1993). Sphingosine-mediated membrane association of DNA and its reversal by phosphatidic acid. *Chem Phys Lipids* **66:** 75-85.

Knorr V, Allmendinger L, Walker GF, Paintner FF, Wagner E. (2007). An acetal-based PEGylation reagent for pH-sensitive shielding of DNA polyplexes. *Bioconjug Chem* **18:** 1218-1225.

Koppel DE. (1972). Analysis of macromolecular polydispersity in intensity correlation spectroscopy: The method of cumulants. *J Chem Phys* **57:** 4814-4820.

Lasic DD. (1996). Doxorubicin in sterically stabilized liposomes. *Nature **380:** 561-562*

Lasic DD. (1988). The mechanism of vesicle formation. *Biochem J* **256:** 1-11.

Lasič DD. (1987). A general model of vesicle formation. *J Theor Biol* **124:** 35-41.

Leventis R, Silvius JR. (1990). Interactions of mammalian cells with lipid dispersions containing novel metabolizable cationic amphiphiles. *Biochim Biophys Acta* **1023:** 124-132.

Li W, Szoka FC,Jr. (2007). Lipid-based nanoparticles for nucleic acid delivery. *Pharm Res* **24:** 438-449.

Ma Z, Wu X, Cao M, Pan W, Zhu F, Chen J *et al.* (2003). Selection of trkB-binding peptides from a phage-displayed random peptide library. *Sci China C Life Sci* **46:** 77-86.

MacDonald RC, MacDonald RI, Menco BP, Takeshita K, Subbarao NK, Hu LR. (1991). Small-volume extrusion apparatus for preparation of large, unilamellar vesicles. *Biochim Biophys Acta* **1061:** 297-303.

Maeda H. (2001). The enhanced permeability and retention (EPR) effect in tumor vasculature: The key role of tumor-selective macromolecular drug targeting. *Adv Enzyme Regul* **41:** 189-207.

Matteucci ML, Thrall DE. (2000). The role of liposomes in drug delivery and diagnostic imaging: A review. *Vet Radiol Ultrasound* **41:** 100-107.

McCall AA, Swan EE, Borenstein JT, Sewell WF, Kujawa SG, McKenna MJ. (2010). Drug delivery for treatment of inner ear disease: Current state of knowledge. *Ear Hear* **31:** 156-165.

McIntyre JC, Sleight RG. (1991). Fluorescence assay for phospholipid membrane asymmetry. *Biochemistry* **30:** 11819-11827.

Nanoear (2011): 3g-Nanotechnology based targeted drug delivery using the inner ear as a model target organ, http://www.nanoear.org (*Last visited 19.8.2012*).

Parry MJ, Hagen M, Mouritsen OG, Kinnunen PK, Alakoskela JM. (2010). Interlamellar coupling of phospholipid bilayers in liposomes: An emergent property of lipid rearrangement. *Langmuir* **26:** 4909-4915.

Paukku T, Lauraeus S, Huhtaniemi I, Kinnunen PK. (1997). Novel cationic liposomes for DNA-transfection with high efficiency and low toxicity. *Chem Phys Lipids* **87:** 23-29.

Plank C, Oberhauser B, Mechtler K, Koch C, Wagner E. (1994). The influence of endosome-disruptive peptides on gene transfer using synthetic virus-like gene transfer systems. *J Biol Chem* **269:** 12918-12924.

Poe DS, Pyykkö I. (2011). Nanotechnology and the treatment of inner ear diseases. *Wiley Interdiscip Rev Nanomed Nanobiotechnol* **3:** 212-221.

Richardson ES, Pitt WG, Woodbury DJ. (2007). The role of cavitation in liposome formation. *Biophys J* **93:** 4100-4107.

Roy S, Johnston AH, Newman TA, Glueckert R, Dudas J, Bitsche M *et al.* (2010). Cell-specific targeting in the mouse inner ear using nanoparticles conjugated with a neurotrophin-derived peptide ligand: Potential tool for drug delivery. *Int J Pharm* **390:** 214-224.

Ryhanen SJ, Saily MJ, Paukku T, Borocci S, Mancini G, Holopainen JM *et al.* (2003). Surface charge density determines the efficiency of cationic gemini surfactant based lipofection. *Biophys J* **84:** 578-587.

Saad SM, Policova Z, Acosta EJ, Hair ML, Neumann AW. (2009). Mixed DPPC/DPPG monolayers at very high film compression. *Langmuir* **25:** 10907-10912.

Saily VM, Ryhanen SJ, Lankinen H, Luciani P, Mancini G, Parry MJ *et al.* (2006). Impact of reductive cleavage of an intramolecular disulfide bond containing cationic gemini surfactant in monolayers and bilayers. *Langmuir* **22:** 956-962.

Schimmang T, Tan J, Muller M, Zimmermann U, Rohbock K, Kopschall I *et al.* (2003). Lack of bdnf and TrkB signalling in the postnatal cochlea leads to a spatial reshaping of innervation along the tonotopic axis and hearing loss. *Development* **130:** 4741-4750.

Shi N, Pardridge WM. (2000). Noninvasive gene targeting to the brain. *Proc Natl Acad Sci U S A* **97:** 7567-7572.

Singh J, Michel D, Chitanda JM, Verrall RE, Badea I. (2012). Evaluation of cellular uptake and intracellular trafficking as determining factors of gene expression for amino acid-substituted gemini surfactant-based DNA nanoparticles. *J Nanobiotechnology* **10:**.

Solodin I, Brown CS, Bruno MS, Chow CY, Jang EH, Debs RJ *et al.* (1995). A novel series of amphiphilic imidazolinium compounds for *in vitro* and *in vivo* gene delivery. *Biochemistry* **34:** 13537-13544.

Spring KR. (1998). Routes and mechanism of fluid transport by epithelia. *Annu Rev Physiol* **60:** 105-119.

Sternberg B, Sorgi FL, Huang L. (1994). New structures in complex formation between DNA and cationic liposomes visualized by freeze-fracture electron microscopy. *FEBS Lett* **356:** 361-366.

Subramanian M, Holopainen JM, Paukku T, Eriksson O, Huhtaniemi I, Kinnunen PK. (2000). Characterisation of three novel cationic lipids as liposomal complexes with DNA. *Biochim Biophys Acta* **1466:** 289-305.

Szoka F,Jr, Papahadjopoulos D. (1978). Procedure for preparation of liposomes with large internal aqueous space and high capture by reverse-phase evaporation. *Proc Natl Acad Sci U S A* **75:** 4194-4198.

Takemura K, Komeda M, Yagi M, Himeno C, Izumikawa M, Doi T *et al.* (2004). Direct inner ear infusion of dexamethasone attenuates noise-induced trauma in guinea pig. *Hear Res* **196:** 58-68.

Thuren T, Virtanen JA, Kinnunen PK. (1986). Estimation of the equilibrium lateral pressure in 1-palmitoyl-2-[6(pyren-1-yl)]hexanoyl-glycerophospholipid liposomes. *Chem Phys Lipids* **41:** 329-334.

Torchilin VP. (2005). Recent advances with liposomes as pharmaceutical carriers. *Nat Rev Drug Discov* **4:** 145-160.

Torchilin VP. (1996). Liposomes as delivery agents for medical imaging. *Mol Med Today* **2:** 242-249.

Torchilin VP. (1993). pH-Sensitive liposomes. *J Liposome Res* **3:** 201-55.

Tsukita S, Furuse M, Itoh M. (1999). Structural and signalling molecules come together at tight junctions. *Curr Opin Cell Biol* **11:** 628-633.

Wagner V, Dullaart A, Bock AK, Zweck A. (2006). The emerging nanomedicine landscape. *Nat Biotechnol* **24:** 1211-1217.

Unger E, Fritz T, Shen DK, Lund P, Sahn D, Ramaswami R *et al.* (1994). Gas filled lipid bilayers as imaging contrast agents. *J Liposome Res* **4:** 861-875.

Walther LE, Westhofen M. (2007). Presbyvertigo-aging of otoconia and vestibular sensory cells. *J Vestib Res* **17:** 89-92.

Wheeler CJ, Sukhu L, Yang G, Tsai Y, Bustamente C, Felgner P *et al.* (1996). Converting an alcohol to an amine in a cationic lipid dramatically alters the co-lipid requirement, cellular transfection activity and the ultrastructure of DNA-cytofectin complexes. *Biochim Biophys Acta* **1280:** 1-11.

WHO website 2012. Available at:
http://www.who.int/mediacentre/news/new/2006/nw01/en
[accessed on 19 August 2012].

WHO 2008, *The World Health Report*. 2008.

Woodbury DJ, Richardson ES, Grigg AW, Welling RD, Knudson BH. (2006). Reducing liposome size with ultrasound: Bimodal size distributions. *J Liposome Res* **16:** 57-80.

Woods C, Montcouquiol M, Kelley MW. (2004). Math1 regulates development of the sensory epithelium in the mammalian cochlea. *Nat Neurosci* **7:** 1310–1318.

Xu Y, Hui SW, Frederik P, Szoka FC,Jr. (1999). Physicochemical characterization and purification of cationic lipoplexes. *Biophys J* **77:** 341-353.

Zhang L, Gu FX, Chan JM, Wang AZ, Langer RS, Farokhzad OC. (2008). Nanoparticles in medicine: Therapeutic applications and developments. *Clin Pharmacol Ther* **83:** 761-769.

Zhang W, Zhang Y, Sood R, Ranjan S, Surovtseva E, Ahmad A *et al*. (2011). Visualization of intracellular trafficking of Math1 protein in different cell types with a newly-constructed nonviral gene delivery plasmid. *J Gene Med* **13:** 134-144.

Zhang Y, Zhang W, Johnston AH, Newman TA, Pyykko I, Zou J. (2010). Improving the visualization of fluorescently tagged nanoparticles and fluorophore-labeled molecular probes by treatment with CuSO(4) to quench autofluorescence in the rat inner ear. *Hear Res* **269:** 1-11.

Zheng JL, Gao WQ. (2000). Overexpression of Math1 induces robust production of extra hair cells in postnatal rat inner ears. *Nat Neurosci* **3:** 580-586.

Zine A, Aubert A, Qiu J, Therianos S, Guillemot F, Kageyama R *et al*. (2001). Hes1 and Hes5 activities are required for the normal development of the hair cells in the mammalian inner ear. *J Neurosci* **21:** 4712-4720.

Zou J, Ramadan UA, Pyykko I. (2010). Gadolinium uptake in the rat inner ear perilymph evaluated with 4.7 T MRI: A comparison between transtympanic injection and gelatin sponge-based diffusion through the round window membrane. *Otol Neurotol* **31:** 637-641.

Zou J, Zhang Y, Zhang W, Ranjan S, Sood R, Mikhailov A *et al*. (2009). Internalization of liposome nanoparticles functionalized with TrkB ligand in rat cochlear cell populations. *Eur J Nanomed* **2:** 7–13.

Aalto-DD 140/2012

Liposome nanoparticles encapsulating therapeutic agents, represent one of the most advanced classes of drug delivery systems, with several currently on the market and many more in clinical trials. According to the World Health Organisation, Inner ear disease is a significant problem, with hearing loss and deafness affected at least 278 million people worldwide. The European Union has ranked hearing impairment in the seventh place on the disability list with more than 60 million citizens affected by hearing loss at an annual cost of 107 billion euros. In this dissertation, a novel method has been developed to prepare liposomes and these liposomes are used to deliver therapeutic or imaging agents to the inner ear of mouse or rat. This work has potential applicability to the development of therapies for disorders of the inner ear.

ISBN 978-952-60-4837-6
ISBN 978-952-60-4838-3 (pdf)
ISSN-L 1799-4934
ISSN 1799-4934
ISSN 1799-4942 (pdf)

Aalto University
School of Science
Department of Biomedical Engineering and Computational Science

BUSINESS + ECONOMY

ART + DESIGN + ARCHITECTURE

SCIENCE + TECHNOLOGY

CROSSOVER

DOCTORAL DISSERTATIONS